



**HAL**  
open science

# From seasonal flood pulse to seiche: Multi-frequency waterlevel fluctuations in a large shallow tropical lagoon (Nokoué Lagoon, Benin)

Alexis Chaigneau, Victor Okpeitcha, Yves Morel, Thomas Stieglitz, Arnaud Assogba, Morgane Benoist, Pierre Allamel, Jules Honfo, Thierry Derol Awoulmbang Sakpak, Fabien Rétif, et al.

## ► To cite this version:

Alexis Chaigneau, Victor Okpeitcha, Yves Morel, Thomas Stieglitz, Arnaud Assogba, et al.. From seasonal flood pulse to seiche: Multi-frequency waterlevel fluctuations in a large shallow tropical lagoon (Nokoué Lagoon, Benin). 2021. hal-03368402

**HAL Id: hal-03368402**

**<https://hal.science/hal-03368402>**

Preprint submitted on 6 Oct 2021

**HAL** is a multi-disciplinary open access archive for the deposit and dissemination of scientific research documents, whether they are published or not. The documents may come from teaching and research institutions in France or abroad, or from public or private research centers.

L'archive ouverte pluridisciplinaire **HAL**, est destinée au dépôt et à la diffusion de documents scientifiques de niveau recherche, publiés ou non, émanant des établissements d'enseignement et de recherche français ou étrangers, des laboratoires publics ou privés.

1 **From seasonal flood pulse to seiche: Multi-frequency water-**  
2 **level fluctuations in a large shallow tropical lagoon (Nokoué**  
3 **Lagoon, Benin).**

4  
5 Alexis CHAIGNEAU<sup>a,b,c,\*</sup>, Victor OKPEITCHA<sup>d,c,b</sup>, Yves MOREL<sup>a</sup>, Thomas STIEGLITZ<sup>e</sup>,  
6 Arnaud ASSOGBA<sup>b</sup>, Morgane BENOIST<sup>a,b</sup>, Pierre ALLAMEL<sup>f</sup>, Jules HONFO<sup>c</sup>, Thierry Derol  
7 AWOULMBANG SAKPAK<sup>g</sup>, Fabien RÉTIF<sup>h</sup>, Thomas DUHAUT<sup>a</sup>, Christophe PEUGEOT<sup>i</sup>,  
8 Zacharie SOHOU<sup>b</sup>

9  
10 <sup>a</sup> Laboratoire d'Études en Géophysique et Océanographie Spatiale (LEGOS), Université de  
11 Toulouse, CNES, CNRS, IRD, UPS, Toulouse, France

12 <sup>b</sup> Institut de Recherches Halieutiques et Océanologiques du Bénin (IRHOB), Cotonou,  
13 Bénin,

14 <sup>c</sup> International Chair in Mathematical Physics and Applications (ICMPA–UNESCO Chair),  
15 University of Abomey-Calavi, Cotonou, Benin

16 <sup>d</sup> Laboratoire d'Hydrologie Appliquée (LHA), Institut National de l'Eau (INE), African  
17 Centre of Excellence for Water and Sanitation (C2EA), Université d'Abomey Calavi, Bénin

18 <sup>e</sup> Aix-Marseille Université, CNRS, IRD, INRAE, Coll France, CEREGE, Aix-en-Provence,  
19 France

20 <sup>f</sup> STATMarine, La Seyne Sur Mer, France

21 <sup>g</sup> Laboratoire des Technologies et Sciences Appliquées, Université de Douala, Douala,  
22 Cameroun

23 <sup>h</sup> RETIF FABIEN PHILIAN, Montferrier sur Lez, France

24 <sup>i</sup> Hydrosiences Montpellier (HSM), Université de Montpellier, CNRS, IRD, Montpellier,  
25 France

26

27

28

29

30 **\*Corresponding Author: alexis.chaigneau@ird.fr**

31

32 **Abstract**

33 This study investigated the main water-level (WL) variability modes of Nokoué  
34 Lagoon in Benin (West-Africa). The average WL ranges between 1.3 and 2.3 m between  
35 the low- and high-water seasons. Seasonal as well as weak interannual variations  
36 between 2018 and 2019 are driven by rainfall regime over the catchment and associated  
37 river inflow. **At sub-monthly scales, the lagoon is tidally choked: ocean tides can reach**  
38 **90 cm, whereas in the lagoon semi-diurnal and diurnal tides hardly reach few**  
39 **centimeters. Choking conditions vary with river inflow and ocean tide amplitude,**  
40 **correctly represented by a simple tidal choking model.** Diurnal modulation and  
41 asymmetry of the tide are stronger (weaker) during high (low) water period. We also  
42 observed WL variations of  $\pm 5$ -10 cm at a fortnightly frequency, stronger during wet  
43 (high-water) season. Superimposed on the seasonal, fortnightly and tidal WL variations,  
44 we further observed short-term high-frequency seiche events. Mostly observed during  
45 dry (low-water) conditions, they are characterized by typical standing-wave oscillations  
46 of 5-10 cm amplitudes and 3 h periods. They are forced by the passage of fast-moving  
47 squall-lines that induce strong wind variations, heavy rainfalls and rapid drop-off of the  
48 air temperature. Results obtained in this study provide useful metrics for the validation  
49 of flood forecasting models to be implemented in Benin, and elsewhere on the West  
50 African coastline.

51

52

53 **Keywords:** Water-levels; Lagoons; Tides; Seiches; Nokoué; Wavelet analysis.

54

55

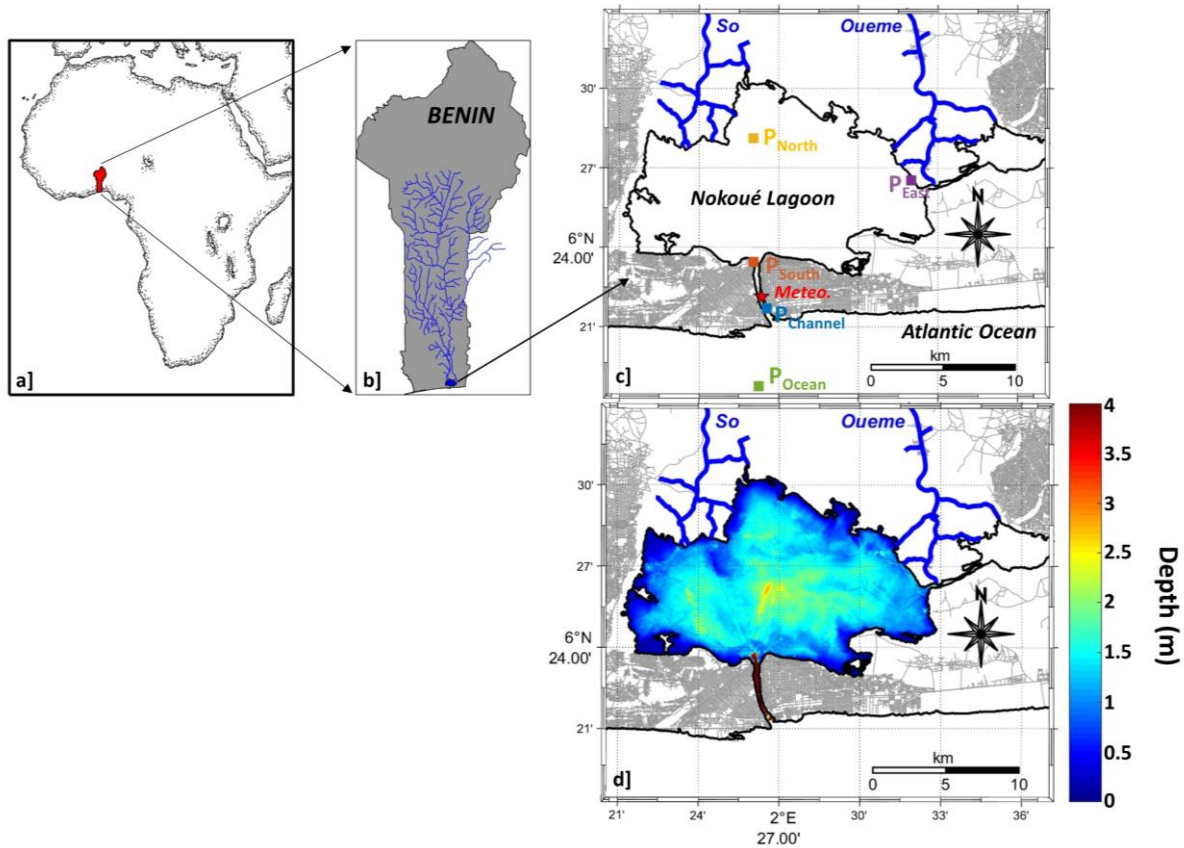
56

## 57 **1. Introduction**

58 In the eastern tropical Atlantic Ocean, the coastal zone bordering the Gulf of  
59 Guinea include a series of coastal lagoons of varying sizes (Allersma and Tilmans, 1993;  
60 Lalèyè et al., 2007; Adite and Winemiller, 1997; Adite et al., 2013). These lagoons are  
61 often the main mixing zone of continental freshwater and coastal seawater, supporting  
62 some of the most productive aquatic ecosystems in the world (Knoppers, 1994; Valiela,  
63 1995; Duck and da Silva, 2012). These coastal systems support important ecosystem  
64 services for the local populations who benefit from these natural or semi-natural areas  
65 through different activities (fishing, tourism, sand and/or salt extraction, etc.)  
66 (Djihouessi et al., 2017; Newton et al., 2018).

67 Among the various Beninese coastal lagoons, Nokoué Lagoon (Figure 1) is the  
68 largest and most exploited of the country's water bodies (Lalèyè et al., 1995; 2003). This  
69 lagoon, which is also one of the most productive in West Africa (Lalèyè et al., 2007), is at  
70 the heart of important ecological and socio-economic issues. It is part of the RAMSAR  
71 site #1018, recognized to be of international importance for its various ecosystems that  
72 include flood plains, mangroves, floating vegetation, and diverse fauna. This lagoon also  
73 hosts several lacustrine villages inhabited by more than 60000 people living in stilt  
74 dwellings (Principaud, 1995). These local populations depend on this water body not  
75 only for fishing, which provides ~15000 tons of fish per year (Principaud, 1995), but  
76 also for domestic water supply, agriculture, market gardening, animal husbandry, etc.  
77 But the Nokoué Lagoon, also bordered by 3 major urban centers (Cotonou, Abomey-  
78 Calavi, and Sémè Podji) totalizing more than 1.5 million inhabitants, is strongly impacted  
79 by various anthropogenic pollution sources. For instance, the lagoon is the receptacle of  
80 numerous urban drains and direct discharge by the surrounding populations of various  
81 wastes which has led to a deterioration of the water quality (Adjahouinou et al., 2012;  
82 2014; Aina et al., 2012a; 2012b). In addition, Nokoué Lagoon is also embedded within  
83 the 500 km long West African coastal water corridor that stretches from Lagos (Nigeria)  
84 to Accra (Ghana). This coastal corridor is projected to become the largest African  
85 urbanized area (Choplin, 2019), a development that will threaten the lagoons'  
86 ecosystems and their service function. The planning and implementation of coastal  
87 management strategies requires a comprehensive knowledge of processes involved in  
88 the physical, chemical and ecological dynamics of the Nokoué Lagoon.

89



90  
91  
92  
93  
94

*Figure 1. Geographical location of the Nokoué Lagoon in Bénin. a) Bénin in West-Africa. b) Hydrological network of the Sô and Ouémé river catchment basins. c) Nokoué Lagoon and position of the water-level stations (colored squares); the location of the weather station is indicated by a red star. d) Bathymetry corresponding to the mean water-level observed in low water season and obtained from a spatial interpolation of ~123000 depth soundings.*

95 One of the key parameters of coastal lagoon dynamics is the water level (WL)  
96 whose variations are mainly subject to the triple influence of (i) ocean tides, (ii) the  
97 hydrological variability of the catchment and (iii) direct rainfall contributions. Generally,  
98 high WL is associated with strong freshwater river discharge and low WL with time  
99 periods when salty oceanic water penetrates into the lagoon. First, WL fluctuations  
100 impact the lagoon circulation and consequently the turnover, residence or flushing times  
101 and therefore the dispersion or retention of pollutants. Second, the lagoon WL  
102 determines the exchange of properties between the continent and the ocean and  
103 controls the ecosystems by various direct or indirect processes. In a direct way, WL  
104 fluctuations control the salinity of the lagoon (e.g. Djihouessi and Aina, 2018), which  
105 directly impacts the ecosystem composition from plankton to fish (Le Barbé et al., 1993;  
106 Gnohossou, 2006; Adandedjan et al., 2017; Odountan et al., 2019; Laléyè et al., 2003;  
107 2005). In an indirect way, WL variations impact lagoon and sediment dynamics by  
108 modifying erosion and sedimentation zones and the rate of sediment resuspension.  
109 Thus, turbidity and the availability of light on the vertical can vary according to the WL,

110 which can modify the structure of biological communities, particularly phytoplankton  
111 (Evtimova and Donohue, 2016). Similarly, WL fluctuations are correlated with  
112 modifications of nutrient concentrations, mixing and vertical stratification in the water  
113 column, eventually affecting the development, distribution and dilution of organisms as  
114 observed in other water bodies (e.g. Lobo et al., 2018; Stević et al., 2013).

115 Third, in addition to having direct or indirect effects on the ecosystem, variations  
116 in the WL of Nokoué Lagoon can have dramatic repercussions on local populations.  
117 Indeed, lacustrine villages and urbanized areas adjacent to the lagoon episodically  
118 experience flooding linked to major watershed floods and the regular overflow of the  
119 lagoon. For instance, in 2010, flooding killed tens of people and affected 360 000, leaving  
120 100 000 homeless (World Bank, 2011; Ahouangan et al., 2014; Biao, 2017). More  
121 recently, in October-November 2019, the floods, less intense but spread over several  
122 weeks, also caused extensive damage and affected tens of thousands of households.

123 Finally, variations in the WL may also impact the quality of the groundwater that  
124 is exploited by residents bordering the lagoon, who use this unregulated shallow  
125 groundwater resource for domestic purposes, including drinking water supplies  
126 (Houéménou et al., 2020).

127 Only few studies described some patterns of WL fluctuations in Nokoué Lagoon  
128 (e.g. Le Barbé et al., 1983; Zandagba et al., 2016; Djihouessi and Aina, 2018). Based on  
129 observations obtained over isolated and short time periods, the WL variability is poorly  
130 described: a seasonal increase of ~50-70 cm is mentioned during the flood season (Le  
131 Barbé et al., 1983; Djihouessi and Aina, 2018) and tidal amplitudes of 10-25 cm were  
132 observed in the Cotonou channel (Zandagba et al., 2016). This study aims to fill this gap  
133 and to investigate WL variations in this lagoon at different time scales from a 2-year in-  
134 situ dataset at 20 min sampling, and to determine the main physical mechanisms  
135 governing the observed fluctuations.

136

## 137 **2. Material and methods**

### 138 **2.1. Study area and hydrology**

139 Nokoué is a costal lagoon that extends about 20 km from east to west along the  
140 coast and 11 km from south to north (Figure 1), covering an average area of ~170 km<sup>2</sup>  
141 (Texier et al., 1980; Le Barbé et al., 1993; Mama et al., 2011; Djihouessi et al., 2019). Two  
142 main rivers flow into the lagoon on its northern shore, the Sô river, draining a relatively

143 small catchment area of  $\sim 1000 \text{ km}^2$ , and the Ouémé river, the largest Beninese river,  
144 which drains a catchment area of  $\sim 50000 \text{ km}^2$  (Le Barbé et al., 1993; Djihouessi et al.,  
145 2017). The Sô and the lower Ouémé valley flow into the Nokoué Lagoon forming a large  
146 flooded deltaic plain (e.g. Le Barbé et al., 1993). A third river, the Djonou, whose  
147 extension and flow are much smaller, also contributes to the freshwater inflow in the  
148 lagoon's southwestern part (Djihouessi and Aina, 2018).

149 On its southern part, Nokoué Lagoon is connected with the Atlantic Ocean by the  
150  $\sim 280 \text{ m}$  wide and  $\sim 4 \text{ km}$  long Cotonou channel (Texier et al., 1980; Le Barbé et al.,  
151 1993). Through this relatively narrow channel, exchanges of fresh and salt water take  
152 place at the rhythm of the tides and the hydrological regime. Since the channel's  
153 construction in 1885, the previously unconnected 'Lake' Nokoué (as it is still known in  
154 colloquial language) is today an extensive lagoon that exhibits important salinity  
155 variations (e.g. Okpeitcha et al., in review).

156 On the eastern side, Nokoué Lagoon is connected to the Porto-Novo lagoon ( $35$   
157  $\text{ km}^2$ ) via the  $\sim 4 \text{ km}$  long Totchè channel. Porto-Novo lagoon extends eastward into a  
158 narrow coastal channel that discharges in the Atlantic Ocean at Lagos (Nigeria) at a  
159 distance of  $\sim 100 \text{ km}$  from Nokoué Lagoon, with little effect on the dynamics and WL of  
160 Nokoué Lagoon (Texier et al., 1980; Le Barbé et al., 1993).

161 On seasonal scales, the lagoon's hydrological regime is driven by the West African  
162 summer monsoon related to the meridional shift of the intertropical convergence zone  
163 (ITCZ) and the associated intense tropical rain belt (Sultan and Janicot, 2000; Gu and  
164 Adler, 2004), resulting in two rainy and two dry seasons. The main rainy season extends  
165 from April-May to late July when the ITCZ moves northward from its near-equatorial  
166 southernmost position, while the second shorter and less intense rainy period extends  
167 from late September to November when the ITCZ migrates southward from its  
168 northernmost position (e.g. N'Tcha M'Po et al., 2017; Ahokpossi, 2018). However, this  
169 double rainy season and associated local rainfalls only slightly influence the WL of the  
170 Nokoué Lagoon that is more subject to the hydrology of the central part of Benin, where  
171 the main area of the Ouémé catchment takes place (e.g. Colleuil, 1987; see also Figure  
172 1b). This latter region is characterized by a single rainy season, with maximum  
173 precipitation between July and October (Biao, 2017; Ahokpossi, 2018; Lawin et al., 2019,  
174 Colleuil, 1987). The maximum discharge into the lagoon between September and  
175 November is unknown (rivers ungauged in the coastal region) and varies, depending on

176 authors, from  $\sim 400 \text{ m}^3 \text{ s}^{-1}$  (Le Barbé et al., 1993; Djihouessi and Aina, 2018) to more  
177 than  $1000 \text{ m}^3 \text{ s}^{-1}$  (Lawin et al., 2019). This river discharge produces a complete  
178 desalinization of the Nokoué Lagoon and a strong increase of its volume (Texier et al.,  
179 1980; Colleuil, 1987; Djihouessi and Aina, 2018).

180 Figure 1d shows the bathymetry of the Nokoué Lagoon corresponding to the  
181 mean WL observed during low-water season in March-April. It was constructed using  
182  $\sim 123000$  depth soundings recorded with a Garmin GPSmap 421S echosounder and  
183 corrected for tidal and seasonal fluctuations. The mean and maximum depth is 1.3 m  
184 and 2.9 m, respectively. The lagoon deepens towards the Cotonou channel where the  
185 mean and maximum depths increase to  $\sim 3$  m and  $\sim 8$  m, respectively (Figure 1d).

186

## 187 **2.2. Water level and atmospheric data**

188 WL data was acquired by 4 pressure sensors deployed in the Cotonou channel  
189 and Nokoué Lagoon for a 2-year period (Figure 1c). Three of them ( $P_{\text{Channel}}$ ,  $P_{\text{South}}$ ,  $P_{\text{North}}$ )  
190 were located along a South-North axis whereas the 4<sup>th</sup> sensor ( $P_{\text{East}}$ ) was deployed East  
191 of the lagoon. More precisely,  $P_{\text{Channel}}$  is located at 1.5 km from the coastal ocean;  $P_{\text{South}}$  is  
192 located at the lagoon entrance;  $P_{\text{North}}$  is located 8.5 km North of  $P_{\text{South}}$  and at  $\sim 2$  km from  
193 the Sô river; finally,  $P_{\text{East}}$  is located 11.3 km southeast of  $P_{\text{North}}$  and 12.3 km northeast of  
194  $P_{\text{South}}$ .

195 Each of the 4 stations consisted of an Onset HOBO U20L-01 WL logger anchored  
196 at 20-30 cm from the bottom in a perforated PVC tube of 7-cm outside diameter. Data  
197 were recorded continuously at 20-min interval between February 2018 and January  
198 2020, with a typical accuracy of  $\pm 1$  cm and a maximum error of 2 cm  
199 ([https://www.onsetcomp.com/files/manual\\_pdfs/17153-G%20U20L%20Manual.pdf](https://www.onsetcomp.com/files/manual_pdfs/17153-G%20U20L%20Manual.pdf))  
200 (Wilson et al., 2016; Guragai et al., 2018).

201 From 30 August 2018, a Davis Vantage Pro2 weather station was installed on the  
202 roof of the Benin Institute of Fisheries and Oceanographic Research (IRHOB; Figure 1c)  
203 also recording at 20-min interval. Some of the atmospheric parameters (air temperature  
204 and humidity, precipitation rates, and winds) are used to explore the forcing  
205 mechanisms involved in high frequency WL variations (Section 3.4). However,  
206 atmospheric pressure data were overall used to correct the WL between September  
207 2018 and January 2020. Before September 2018, WL was not corrected for barometric  
208 fluctuations, but this does not significantly alter the results and main conclusions drawn

209 in this study. Indeed, atmospheric pressure, that varied between 1004 mbar and 1019  
210 mbar over the available time period, exhibits two main modes of variability. First, at  
211 seasonal scale, atmospheric pressure varies by  $\sim 4$  mbar, being minimum in April and  
212 maximum in August. This corresponds to a WL correction of  $\sim 4$  cm which is weak  
213 compared with the seasonal WL variations of  $\sim 90$  cm observed in this study (Section  
214 3.1). Second, the stronger atmospheric pressure variability is observed at diurnal and  
215 semi-diurnal periodicities, with mean and maximum variations of  $\sim 3$  and 6 mbar,  
216 respectively. This corresponds to WL variations of  $\sim 3$ -6 cm, of the same order than the  
217 tidal amplitudes observed in the lagoon. Thus, the tide characteristics in the lagoon  
218 (Section 3.3), are investigated using WL data corrected from inverse barometer effects  
219 (September 2018-December 2019).

220 Raw pressure data are converted to relative WLs corresponding to the height  
221 above the instrument. For each station, as no absolute vertical datum exists, the relative  
222 WLs are expressed in terms of anomalies, computed by subtracting the 20-min  
223 measurements from the seasonal mean calculated over low-water period of 2018.

224 No continuous in-situ ocean tide data is available. We therefore used the tidal  
225 heights computed from the last Finite Elements Solution for ocean tide (FES2014) on a  
226  $1/16^\circ \times 1/16^\circ$  grid ([http://www.aviso.altimetry.fr/en/data/products/auxiliary-](http://www.aviso.altimetry.fr/en/data/products/auxiliary-products/global-tide-fes.html)  
227 [products/global-tide-fes.html](http://www.aviso.altimetry.fr/en/data/products/auxiliary-products/global-tide-fes.html)) (Carrere et al. 2016; Lyard et al. 2020). Thus, WL  
228 anomaly timeseries at  $P_{\text{Ocean}}$  (Figure 1c) was reconstructed using the 34 tidal  
229 constituents (amplitudes and phases) computed from FES2014.  $P_{\text{Ocean}}$  is located  $\sim 5.5$  km  
230 to the southeast of  $P_{\text{Channel}}$  (Figure 1c). FES WL at  $P_{\text{Ocean}}$  compared well with independent  
231 but irregular in-situ WL data acquired at the autonomous port of Cotonou in 2018-2019  
232 by its hydrographic service. The correlation coefficient, mean difference, normalized  
233 root-mean-square error, and ratio of standard deviations between both datasets are  
234 0.99, 0.02 cm, 2.7%, and 0.99, respectively.

235

### 236 **2.3. Rainfall and river discharge data**

237 Rainfall over the catchment was obtained from a Global Precipitation  
238 Measurement (GPM) Integrated Multi-satellitE Retrievals for GPM (IMERG) product  
239 (Huffman et al., 2014). We use the final Level 3 product developed for research  
240 applications, which is available daily on a  $0.1^\circ \times 0.1^\circ$  longitude/latitude grid  
241 (<https://gpm.nasa.gov/>). Rainfall was extracted over the study period (2018-2019) and

242 averaged in the river catchment area shown in Figure 1b. In order to filter out high  
243 frequency variability irrelevant to our study, we used monthly cumulative rainfall.

244 Historical estimates of the Ouémé River discharge at Bonou (~70 km upstream  
245 from the Nokoué Lagoon) and the Sô river discharge at Sô-Awa (~3 km upstream from  
246 the lagoon) are available. These daily data, available from the 1950's to the 1990's, were  
247 collected by the general Benin Directorate of water and made available by the Système  
248 d'Informations Environnementales sur les Ressources en Eau et Modélisation (SIEREM:  
249 <http://www.hydrosciences.org/spip.php?article1236>). A daily climatology was  
250 constructed from this multi-year dataset and the Sô and Ouémé discharges were  
251 summed to provide an estimate of the total fresh water discharge into the lagoon.

252

#### 253 **2.4. Time series analyses**

254 The variability of the WL across temporal scales was investigated using a wavelet-  
255 based analysis (Torrence and Compo, 1998; Guo et al., 2015). The wavelet power  
256 spectrum, that estimates the spectral characteristics of the WL signal as a function of  
257 time, is computed here using the Morlet wavelet transform. In order to compare spectral  
258 peaks across different scales, the obtained wavelet power spectra, that are slightly  
259 biased, are rectified normalizing them by the local scale (Liu et al., 2007; Veeda et al.,  
260 2012). Wavelet decomposition can also be used for signal reconstruction and filtering  
261 (Torrence and Compo, 1998). By summing over a subset of scales, we here construct WL  
262 wavelet-filtered time series in several spectral bands, from high-frequency (periods <  
263 5h) to subtidal and low-frequency (periods > 20 days) variability.

264 **Global power spectra obtained from wavelet analyses provide consistent estimation**  
265 **of the true power spectra computed from Fourier analyses (Percival, 1995). However,**  
266 **due to the width of the wavelet filter in Fourier space, any close peaks in Fourier spectra**  
267 **could be smoothed out by the wavelet analysis, particularly at small (high-frequency)**  
268 **wavelet scales (Hudgins et al., 1993; Torrence and Compo, 1998). Thus, in order to**  
269 **resolve close principal tidal constituents, their mean amplitudes and phases (e.g. Table**  
270 **1) are obtained from harmonic analyses using T\_TIDE package in MATLAB for each time**  
271 **series (Pawlowicz et al., 2002). The temporal evolution of tidal amplitudes is**  
272 **subsequently investigated in the diurnal (D1), semi-diurnal (D2), and quarter-diurnal**  
273 **(D4) spectral bands by integrating wavelet power in these specific frequency/period**  
274 **bands and converting them into wavelet amplitudes as in Guo et al. (2015). The D1, D2**

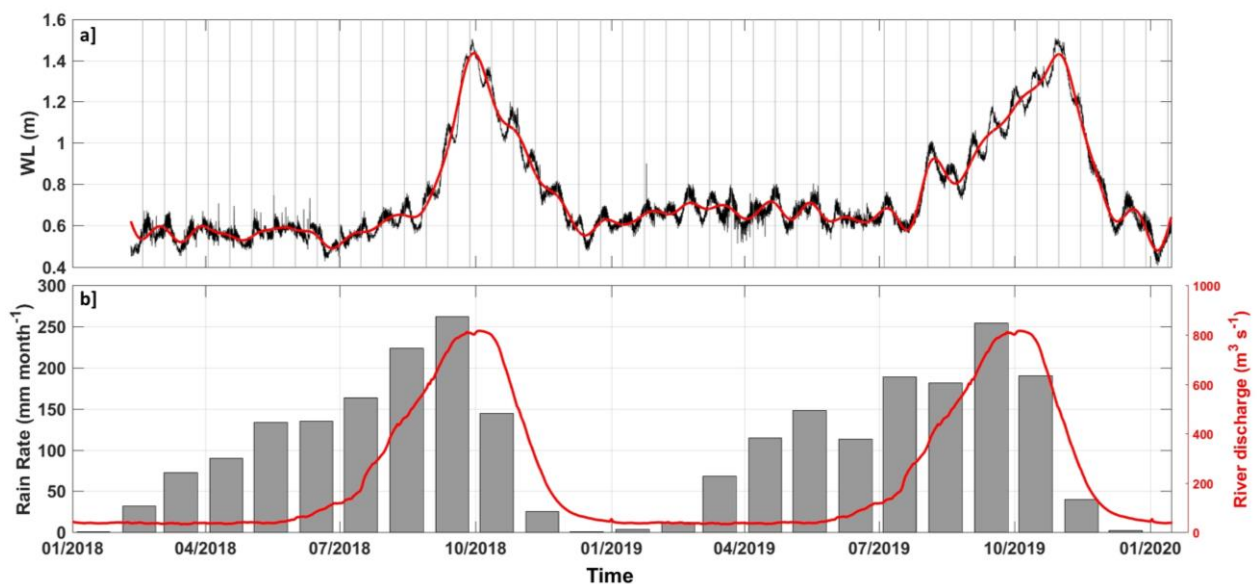
275 and D4 amplitudes are computed for periods of 15-36h, 7.5-15h and 5-7.5h,  
276 respectively.

277

### 278 3. Results

#### 279 3.1. Low-frequency variations

280 At the entrance of the Nokoué Lagoon at  $P_{\text{South}}$ , in the periods from February to  
281 August 2018 and from December 2018 to July 2019, the lagoon WL was low at mean WL  
282 of 0.5-0.6 m in 2018 and 0.6-0.7 m in 2019 (Figure 2a). These periods coincide with  
283 climatological periods when rivers are at baseflow and have discharges of less than  $\sim 50$   
284  $\text{m}^3/\text{s}$  (Figure 2b). From 20 August 2018 to 30 September 2018, the mean WL increased  
285 to reach a maximum value of  $\sim 1.4$  m (Figure 2a). The peak observed in 2018 coincides  
286 with the maximum climatological river discharges of  $\sim 800$   $\text{m}^3/\text{s}$  at the beginning of  
287 October. The decrease of the lagoon WL from 1.4 m to less than 0.6 m was observed  
288 between early October and early December 2018. The duration of the decrease was  
289 comparable to that of the WL rise. In contrast, the duration of increasing/decreasing WL  
290 were strongly asymmetric in 2019. The flooding phase began in late July 2019 and took  
291 3 months to reach the maximum of  $\sim 1.4$  m on 31 October 2019. Although the beginning  
292 of the flooding phase in 2019 approximately follows the climatological river discharge,  
293 the maximum WL was observed 1 month later than the average peak of the hydrograph.  
294 In 2019, the decrease of the lagoon WL took only 1 month, and the low-WL was reached  
295 at the beginning of December, as in 2018.



296

297 *Figure 2. Water-level and hydrological variations. a) Temporal variations of the water-level (WL) at  $P_{\text{South}}$ ; red line shows*  
298 *the low-frequency component associated with periods longer than 20 days where grey vertical lines correspond to the*

299 *time of oceanic spring tides. b) Monthly cumulative rainfall over the Ouémé river catchment basin (grey bars) and*  
300 *estimated climatological river discharge (red line).*

301

302 The monthly cumulative rainfall inferred from satellite data in the Sô and Ouémé  
303 catchment basins do not show strong differences between the time periods of the rainy  
304 season of 2018 and 2019 (Figure 2b). In both 2018 and 2019, the maximum rainfalls  
305 occurred in September. However, October 2019 was 35% rainier (~190 mm) than  
306 October 2018 (~140 mm), which explains the 1-month delay observed in 2019 on the  
307 maximum WL (Figure 2a). Similarly, heavy rainfalls (~190 mm) observed in July 2019,  
308 are responsible for the earlier rise in WL in 2019, as well as for the local maximum  
309 elevation of ~0.95 m observed at the beginning of August 2019. Heavy rainfalls in July-  
310 August 2019 also contributed to spread out the flooding phase and delay the flood peak  
311 in the lagoon.

312 Low-frequency WL variations of the Nokoué Lagoon are related to the rainfall in  
313 the catchment basin and the river flows that discharge fresh water into the lagoon.  
314 However, superimposed on these low-frequency fluctuations, Figure 2a shows that the  
315 unfiltered WL signal exhibits high-frequency variability patterns. The main goal of the  
316 following Sections is thus to investigate these distinct modes of variability.

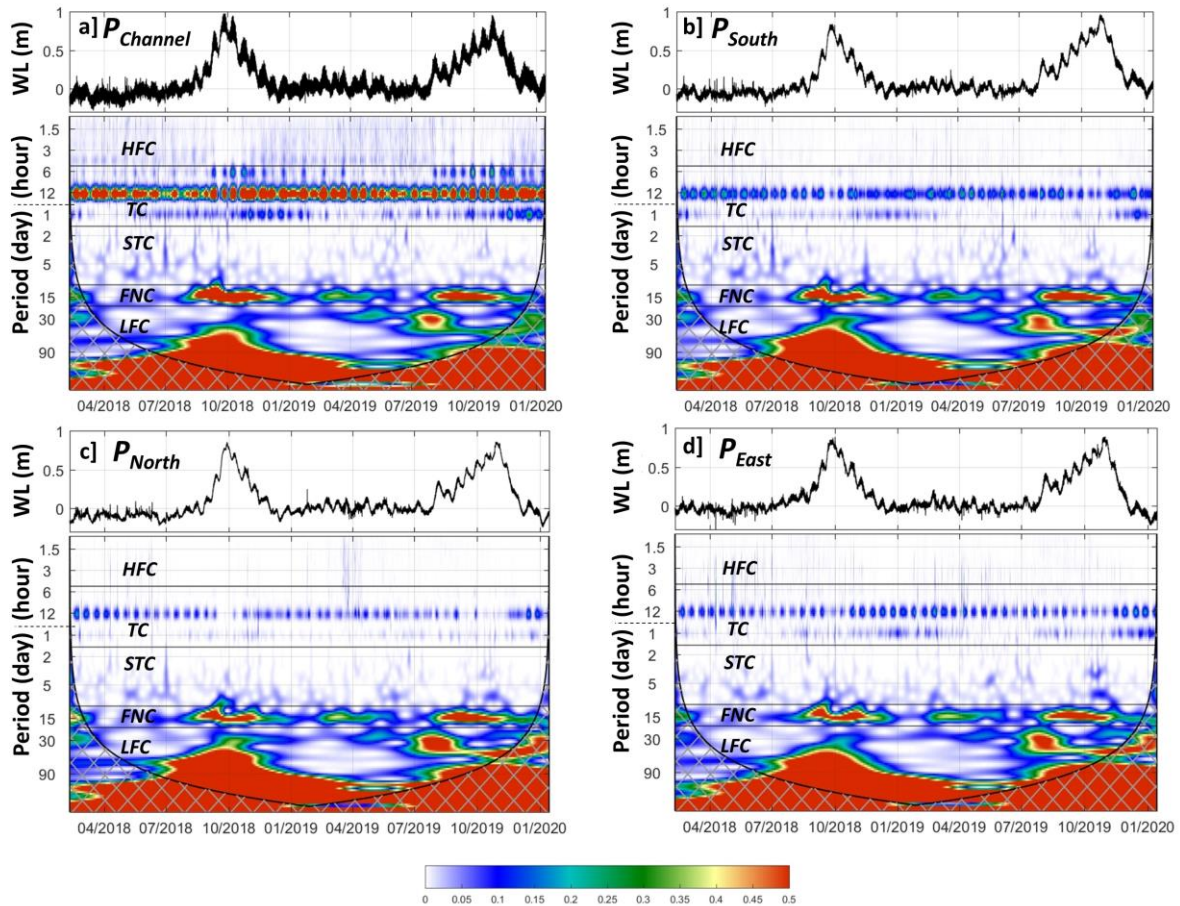
317

### 318 **3.2. WL Wavelet analysis**

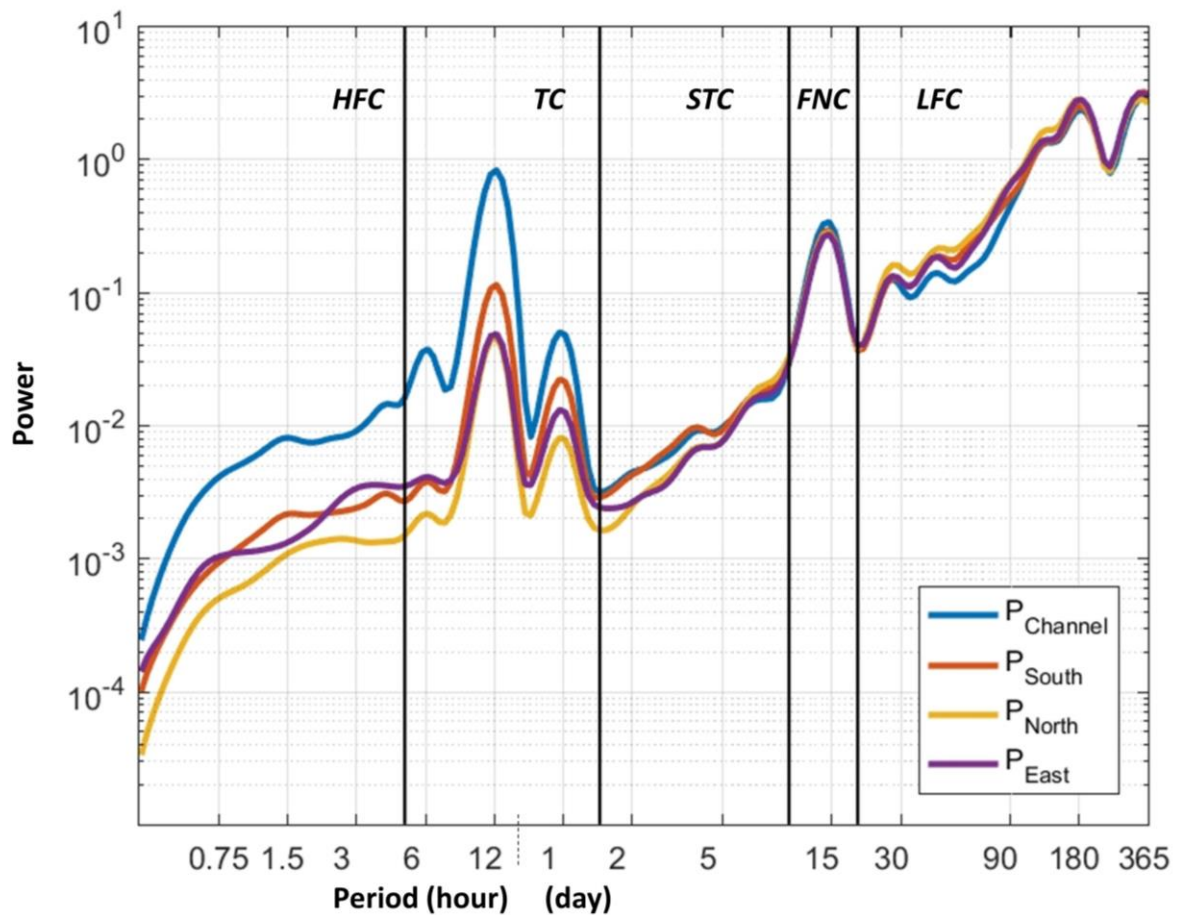
319 During the 2-year period, the 4 WL timeseries show similar patterns, not only at  
320 low-frequency (Figure 3). Superimposed on the already described low frequency WL  
321 variations, higher frequency WL variations with typical ranges of  $\sim\pm 20$  cm that decrease  
322 from the Cotonou channel to the Nokoué Lagoon are evident (Figure 3). In order to  
323 better identify the dominant frequencies, we performed a wavelet analysis (Figures 3  
324 and 4). WL timeseries show time-dependent variability with contributions from distinct  
325 frequency bands at certain times. Spectra can be divided into 5 main period bands, from  
326 high to low frequencies: i) high-frequency component with periods shorter than 5  
327 hours; ii) tidal component with periods ranging between 5 hours and 1.5 days; iii)  
328 subtidal component with periods of 1.5-10 days; iv) fortnightly component with periods  
329 of 10–20 days; and v) low-frequency component with periods longer than 20 days.

330 The low-frequency component has been described in Section 3.1 and  
331 corresponds to large WL variations mainly due to rainfall in the catchment basins that

332 drives the seasonal change in river discharge into the lagoon. In contrast, the subtidal  
 333 component does not present significant spectral energy (Figures 3 and 4) and is thus not  
 334 further investigated. Fortnightly, tidal and high-frequency components are described in  
 335 more detail.  
 336



337  
 338 *Figure 3. Water-level (WL, in m) timeseries and corresponding rectified continuous wavelet power spectra, at a)  $P_{Channel}$ ,*  
 339 *b)  $P_{South}$ , c)  $P_{North}$ , and d)  $P_{East}$ . The rectified wavelet power is  $\log_2(A^2/s)$ , where  $A$  is the wavelet coefficient amplitude, and*  
 340  *$s$  the scale it associates (Liu et al., 2007). The y axis is on a  $\log_2$  scale and in day (hour, respectively) for periods higher*  
 341 *(lower) than 1 day. The cone of influence is indicated by hatched area by 95% confidence level due to the edging effects.*  
 342 *Horizontal black lines on the wavelet spectra delimit 5 frequency bands: High-frequency component (HFC) (periods < 5*  
 343 *hours); Tidal component (TC) (5-36 hours); Subtidal component (STC) (1.5-10 days); Fortnightly component (FNC) (10-*  
 344 *20 days); Low-frequency component (LFC) (> 20 days).*



345  
 346 *Figure 4. Global wavelet power spectra obtained by averaging over time the wavelet power spectrum at a)  $P_{Channel}$ , b)*  
 347  *$P_{South}$ , c)  $P_{North}$ , and d)  $P_{East}$ . Vertical black lines delimit the 5 frequency bands detailed in Figure 4.*

348

### 349 **3.3. Fortnightly and tidal components**

#### 350 **a) Harmonic Analysis and main tidal constituents**

351 Figures 3 and 4 show relatively strong spectral energy in the fortnightly (MSf)  
 352 component. These oscillations of a period of  $\sim 14.8$  days on the mean WL are associated  
 353 with neap and spring tides. Indeed, the combination of the principal lunar (M2) and  
 354 solar (S2) semidiurnal tidal constituents, characterized by very close periods (Table 1),  
 355 induces a compound tide (MSf) and fortnightly variation of the oceanic semi-diurnal tide  
 356 amplitude (e.g. LeBlond, 1979; Pugh, 1987). In the open-ocean, where the mean WL  
 357 variations are weak compared to the tidal range, both the highest and lowest sea-levels  
 358 are observed during spring tides, and the mean WL is not significantly modulated at MSf  
 359 frequencies (Table 1). In contrast, in shallow lagoons or estuaries, complex non-linear  
 360 interactions between oceanic semi-diurnal tides, river fluxes, bottom friction and  
 361 morphology of the channel, result in MSf variations of the WL (LeBlond, 1979; Gallo and  
 362 Vinzon, 2005; Guo et al., 2015). These MSf variations are observed in the Cotonou

363 channel and Nokoué Lagoon (Table 1), where the highest high-waters are observed  
364 during spring tides whereas the lowest low-waters are observed during neap tides  
365 (Figures 2a and 3). This is due to the fact that the tidal amplitude is generally weaker  
366 than the fortnightly variations of the mean WL (Figures 2a and 3; Table 1) induced by  
367 tidal-river interaction processes (e.g. LeBlond, 1979; Guo et al., 2015). Harmonic  
368 analyses indicate a mean MSf amplitude of  $\sim 4$  cm (Table 1), which strongly increases to  
369 10-15 cm during the wet season (not shown but see the evolution of the fortnightly  
370 component in Figure 3).

371 In the open-ocean off Cotonou, tides are semi-diurnal with a relatively important  
372 diurnal component (Table 1). Semi-diurnal tide constituents ( $A_{M2}+A_{S2}$ ) are typically of  
373  $\sim 70$  cm amplitude whereas diurnal constituents ( $A_{O1}+A_{K1}$ ) are of  $\sim 15$  cm. As a result,  
374 the tidal form factor,  $F = \frac{A_{O1}+A_{K1}}{A_{M2}+A_{S2}}$ , which is the amplitude ratio of the diurnal to semi-  
375 diurnal tide constituents, is of 0.22, close to the mixed-tide threshold of 0.25 (Courtier,  
376 1938). Off Cotonou, the tide is thus of semi-diurnal-dominant type, but characterized by  
377 two slightly unequal high and low tides per day. In the Cotonou channel and Nokoué  
378 Lagoon, tidal ranges are strongly dampened and the tidal form factor increases to 0.41  
379 (Table 1). This suggests a stronger modulation of the tides at diurnal scale in the lagoon  
380 and a stronger attenuation of the semi-diurnal constituents compared to the diurnal  
381 constituents.

382 In shallow water, the progression of a tidal wave is modified by bottom friction  
383 and other physical processes that lead to the distortion and asymmetry of the tidal wave  
384 (Pugh et al., 1987). These non-linear effects are associated with the generation of higher  
385 harmonics such as the main M4 constituent, which is the second harmonic (or overtide)  
386 of the principal lunar tide M2, that causes disparities in the rising and falling times (e.g.  
387 Pugh et al., 1987; Gallo and Vinzon, 2005; Ray, 2007). Thus, tidal wave deformation and  
388 asymmetry are mainly due to M2-M4 interactions (e.g. Friedrichs and Aubrey, 1988;  
389 Speer and Aubrey, 1985). The general flood-dominated character of the lagoon system is  
390 highlighted by the phase difference of  $2\varphi_{M2} - \varphi_{M4}$  in the range of  $0-90^\circ$  that leads to a  
391 longer falling tide than rising tide (Friedrichs and Aubrey, 1988; Guo et al., 2015). The  
392 magnitude of the amplitude ratio of the M4 and M2 components ( $\frac{A_{M4}}{A_{M2}}$ ) is an indicator of  
393 the strength of the tidal asymmetry. This factor is of 0.02 at  $P_{Ocean}$  where the tide is

394 symmetric, but increases to 0.11-0.15 in the lagoon system indicating a stronger  
 395 asymmetry and, on average, a deformation of the tidal wave (Table 1).

396

397 *Table 1. Average tidal properties: Tidal amplitudes (A) and phases ( $\varphi$ ) of major diurnal (D1), semi-diurnal (D2),  
 398 quarter-diurnal tides (D4) and fortnightly (FNC) components' frequencies at  $P_{\text{Ocean}}$ ,  $P_{\text{Channel}}$ ,  $P_{\text{South}}$ ,  $P_{\text{North}}$  and  $P_{\text{East}}$ .  
 399 These average tidal constituent properties were determined by harmonic analyses of 2-year WL timeseries using  
 400 T\_TIDE (Pawlowicz et al., 2002). Periods are in hours, except for FNC frequencies where they are in days.*

		Period	$P_{\text{Ocean}}$		$P_{\text{Channel}}$		$P_{\text{South}}$		$P_{\text{North}}$		$P_{\text{East}}$	
			A (cm)	$\varphi$ ( $^{\circ}$ )	A (cm)	$\varphi$ ( $^{\circ}$ )	A (cm)	$\varphi$ ( $^{\circ}$ )	A (cm)	$\varphi$ ( $^{\circ}$ )	A (cm)	$\varphi$ ( $^{\circ}$ )
FNC	MSf	14.77	0.0	125	4.2	60	3.9	66	4.0	70	3.9	69
	Mf	13.66	0.0	96	1.6	55	1.3	63	1.4	60	1.3	60
D1	O1	25.82	2.6	318	0.3	119	0.2	159	0.2	177	0.2	181
	P1	24.07	3.8	346	0.4	45	0.2	78	0.1	81	0.1	60
	S1	24.00	0.1	91	1.0	110	1.0	115	0.2	186	0.4	144
	K1	23.93	12.5	1	1.4	35	0.6	89	0.5	115	0.7	112
D2	N2	12.66	10.8	101	1.5	130	0.5	153	0.3	217	0.3	222
	M2	12.42	50.8	105	7.5	134	2.7	156	1.5	221	1.6	232
	S2	12.00	17.8	130	1.8	167	0.6	241	0.7	299	0.6	306
	K2	11.97	4.3	144	0.8	184	0.3	196	0.2	253	0.2	265
D4	M4	6.21	1.3	319	1.1	266	0.3	280	0.2	16	0.2	18
	MS4	6.10	0.0	104	0.7	288	0.2	299	0.1	53	0.1	48

401

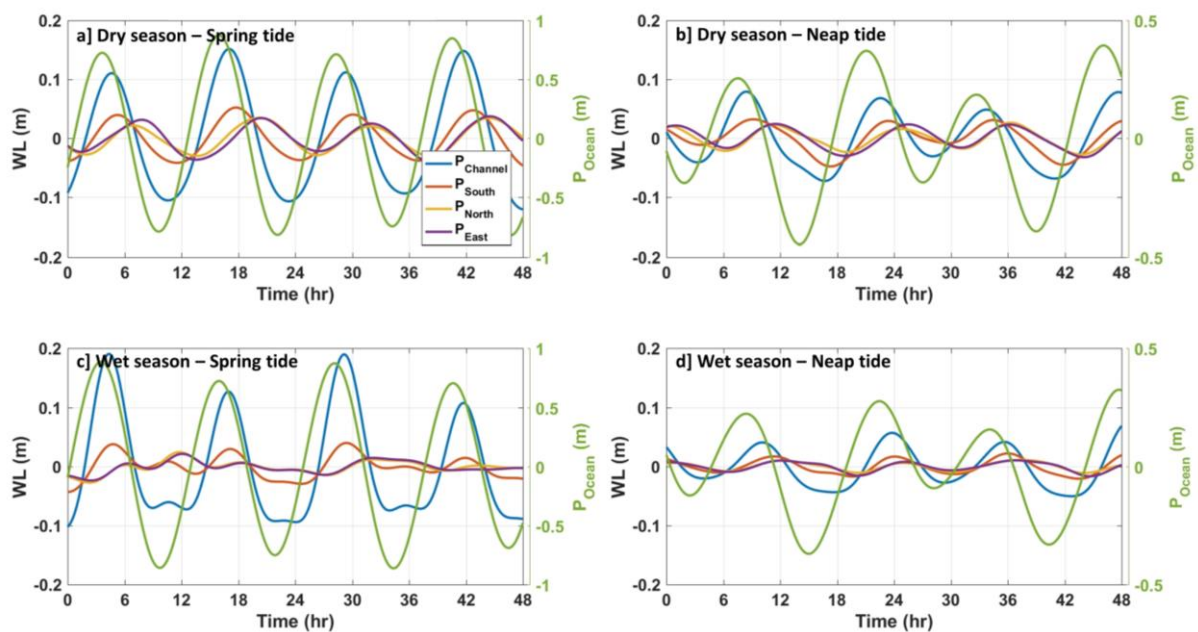
402

### 403 **b) Tidal WL fluctuations during dry/wet seasons and spring/neap tides**

404 Figure 5 shows two-day snippets of WL fluctuations during the dry and wet  
 405 seasons (April and October, respectively) and for different phases of spring-neap tidal  
 406 cycles. During dry season spring tides (Figure 5a), the maximum tidal amplitude is of  
 407 ~80-90 cm in the ocean. It decreases to ~10-15 cm in the Cotonou channel and ~3-5 cm  
 408 in the lagoon. During this period, the average diurnal tidal amplitude (AD1) is of ~15 cm  
 409 in the offshore ocean and of 1-2.5 cm in the lagoon (Table 2). Similarly, the average  
 410 semi-diurnal tidal amplitude (AD2) varies from ~90 cm at  $P_{\text{Ocean}}$  to ~3-15 cm at the  
 411 other stations (Table 2). The AD1/AD2 ratio is 0.1-0.3, suggesting that the tide is mainly  
 412 semidiurnal without strong diurnal modulation, as seen in Figure 5a. Both the quarter-  
 413 diurnal amplitude (AD4) and the AD4/AD2 ratio are weak and the tide appears mostly  
 414 symmetric, without strong deformation.

415 During dry season neap tides (Figure 5b), the minimum tidal amplitude is of ~20  
 416 cm at  $P_{\text{Ocean}}$  but is strongly modulated at diurnal scale. The AD1 amplitude is ~18 cm and

417 AD2 decreased to  $\sim 36$  cm leading to a relatively strong AD1/AD2 ratio of 0.5 (Table 2).  
 418 In the lagoon, tidal amplitudes decrease to  $\sim 1$ -2 cm for AD1 and to 2-7 cm for AD2.  
 419 These values are weaker but the associated AD1/AD2 ratios (0.3-0.7) are slightly higher  
 420 to what was observed during spring tides (Figure 5a-b and Table 2). In the Cotonou  
 421 channel and Nokoué Lagoon during dry season, the rising and falling tidal durations are  
 422 slightly unequal and the tide is only very slightly asymmetric, as indicated by weak AD4  
 423 values of 0.1-0.2. Indeed, the ebb-tide lasts  $\sim 30$ -45 mn longer than the flood-tide, hence  
 424 the lagoon system tends to be flood-dominated (e.g. Speer et al., 1991).  
 425



426  
 427 *Figure 5. Examples of water-level evolution in the tidal frequency band (periods of 5-36 hr) during a) a dry season spring*  
 428 *tide, b) a dry season neap tide, c) a wet season spring tide, d) a wet season neap tide. Water levels (WL, in m) in the*  
 429 *Cotonou channel ( $P_{Channel}$ ) and Nokoué Lagoon ( $P_{South}$ ,  $P_{North}$ ,  $P_{East}$ ) correspond to left axes whereas WL in the ocean*  
 430 *( $P_{Ocean}$ ) correspond to right axes (and green lines).*

431  
 432 During the wet season, the tide characteristics in the open ocean are similar to  
 433 the dry season, with AD1 of  $\sim 15$  cm and AD2 varying from  $\sim 95$  cm for spring tides to  
 434  $\sim 30$  cm for neap tides (Figure 5c-d and Table 2). In contrast, tide characteristics are  
 435 significantly modified in the channel and the lagoon, and more particularly during wet  
 436 season spring tides (Figure 5c). AD2 decreases during wet season and AD1 tends to  
 437 increase (see also wavelet power spectra in Figure 3). The tidal form factor AD1/AD2  
 438 increases from  $\sim 0.1$ -0.7 during the dry season, to 0.5-2.2 during the wet season (Table  
 439 2), as a result of a stronger modulation of the tides at diurnal scale during high water  
 440 periods. During spring tides (Figure 5c), the flood duration is 4-5 h, whereas the ebb-

441 tide lasts 7-8 h. **Notably** the wave shape of the tides tends to be positively skewed with a  
 442 slack-tide asymmetry, in particular at  $P_{\text{Channel}}$  (blue line in Figure 5c). This slack-tide  
 443 asymmetry is due to a phase difference between M2 and M4 ( $2\phi_{\text{M2}} - \phi_{\text{M4}}$ ) that is, on  
 444 average, close to  $0^\circ$  (Table 1) (e.g. Guo et al., 2019).

445 Finally, high and low tides are systematically observed 1 hour later at  $P_{\text{Channel}}$  than  
 446 at  $P_{\text{Ocean}}$  (Figure 5). In contrast, the high or low tide phase shift between  $P_{\text{South}}$  and  $P_{\text{North}}$   
 447 or  $P_{\text{East}}$ , varies from 1h-3h during dry season (Figure 5a,b) and is strongly uncertain  
 448 during wet season when the tide is much more asymmetric and deformed (Figure 5c,d).  
 449 Note also that winds can impact WL in shallow lagoons, in particular by pushing and  
 450 piling up water in the downwind direction (e.g. Stieglitz et al., 2013; Colvin et al., 2018).  
 451 However, data from the weather station reveals that the dominant southwest wind is  
 452 weak and varies from  $2.2 \text{ m s}^{-1}$  in December to  $4.5 \text{ m s}^{-1}$  in August. Similarly, at diurnal  
 453 scale, the wind only varies by  $2 \text{ m s}^{-1}$ , being minimum at 6-7 am and maximum at 3-4  
 454 pm. **Considering a steady state balance between the wind-stress and the barotropic**  
 455 **pressure gradient generated by the slope of the free surface, these typical winds would**  
 456 **result on wind setups of  $\sim 1\text{-}3 \text{ cm}$  in the northeastward direction (see equations in e.g.**  
 457 **Colvin et al., 2018).** This weak signal could not be evidenced in the WL dataset, and no  
 458 significant WL slope was observed between  $P_{\text{North}}/P_{\text{East}}$  and  $P_{\text{South}}$ , neither at seasonal  
 459 nor diurnal scales. However, as described in the following Section, high-frequency  
 460 fluctuations of the wind field generate high-frequency variations of the WL slope in  
 461 Nokoué Lagoon.

462  
 463 *Table 2. Average tidal amplitudes of diurnal (AD1), semi-diurnal (AD2), and quarter-diurnal tides (AD4) at  $P_{\text{Ocean}}$ ,  $P_{\text{Channel}}$ ,  
 464  $P_{\text{South}}$ ,  $P_{\text{North}}$  and  $P_{\text{East}}$  and for 4 selected 48-hour periods. Amplitude ratios (AD1/AD2 and AD2/AD4) are also indicated.  
 465 These average tidal constituent properties were determined by integrating wavelet powers in specific frequency/period  
 466 bands (15-36h for D1, 7.5-15h for D2, and 5-7.5h for D4). Amplitudes are in cm.*

467

	$P_{\text{Ocean}}$	$P_{\text{Channel}}$	$P_{\text{South}}$	$P_{\text{North}}$	$P_{\text{East}}$
<i>Dry Season – Spring Tide</i>					
AD1	13.3	2.6	0.9	1.0	1.0
AD2	94.2	14.2	5.1	3.4	3.5
AD4	3.8	2.0	0.6	0.3	0.4
AD1/AD2	0.14	0.18	0.17	0.30	0.29
AD4/AD2	0.04	0.14	0.12	0.10	0.11
<i>Dry Season – Neap Tide</i>					
AD1	17.6	3.1	2.2	0.6	1.1
AD2	36.0	6.7	3.2	2.4	2.7

468	AD4	1.9	1.2	0.5	0.4	0.3
469	AD1/AD2	0.49	0.47	0.70	0.26	0.42
	AD4/AD2	0.05	0.18	0.15	0.18	0.13

470

471

*Wet Season – Spring Tide*

471	AD1	14.9	3.3	1.8	1.5	1.5
472	AD2	95.3	14.0	2.7	0.7	0.7
	AD4	3.8	5.7	1.5	0.8	0.7
	AD1/AD2	0.16	0.24	0.68	2.06	2.24
	AD4/AD2	0.04	0.41	0.57	1.02	1.01

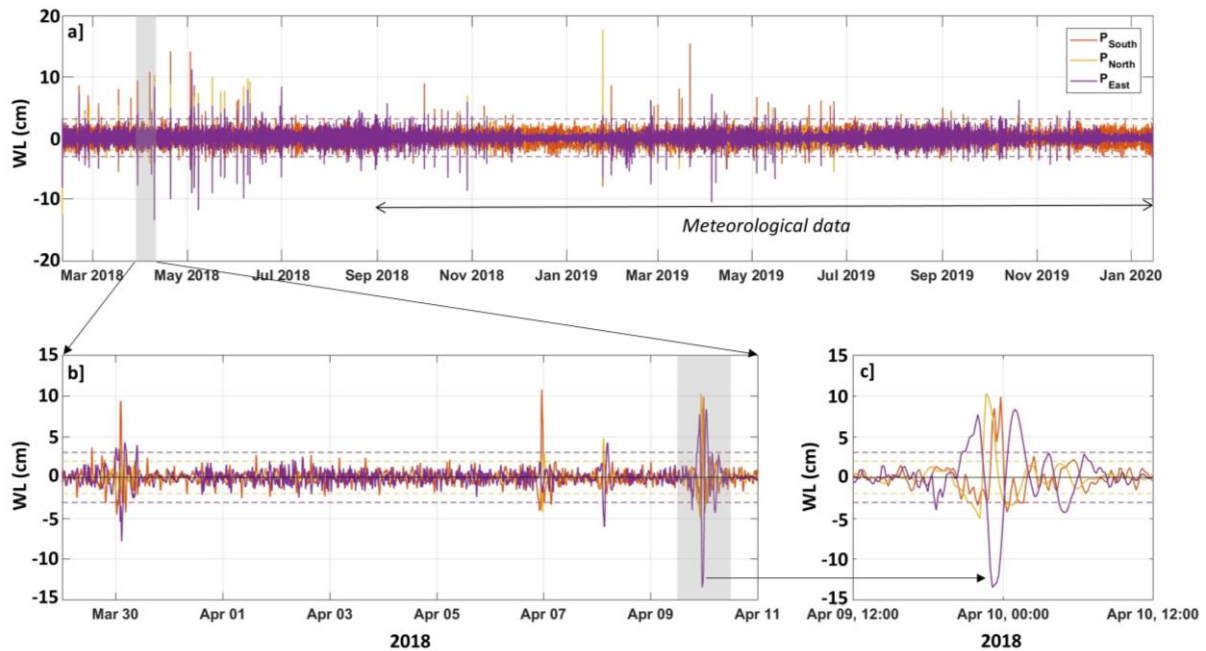
*Wet Season – Neap Tide*

	AD1	16.6	2.1	0.6	0.5	0.6
	AD2	28.0	5.1	1.9	1.0	1.1
	AD4	1.7	1.0	0.5	0.2	0.3
	AD1/AD2	0.59	0.41	0.34	0.54	0.53
	AD4/AD2	0.06	0.21	0.24	0.21	0.28

---

473 **3.4. High-frequency component (periods < 5 hours)**

474 Relatively strong HF variability was observed between February and June 2018,  
475 October-November 2018, and February to June 2019 (Figure 6a). For example, during a  
476 2-week period in 2018, 4 individual HF events were observed (Figure 6b). These high-  
477 frequency fluctuations can be either in phase or in opposition between the different  
478 stations. Typical oscillations of  $\pm 5$ -10 cm are observed.  
479



480  
481 *Figure 6. High-frequency component (HFC) of the water level evolution in the Nokoué Lagoon ( $P_{South}$ ,  $P_{North}$ ,  $P_{East}$ ). a) HFC*  
482 *(periods < 5 hours) for the 2-year study period (2018-2019), showing strong high-frequency events. b) HFC for a 12-day*  
483 *period in April 2018. c) zoom for a particular high-frequency event observed in April 10, 2018. In these figures, horizontal*  
484 *dashed lines correspond to  $\pm 4$  standard deviations around the mean and are used to automatically detect high-frequency*  
485 *events associated with seiches. The period with available meteorological data (September 2018-January 2020) is also*  
486 *indicated by a black arrow in a).*

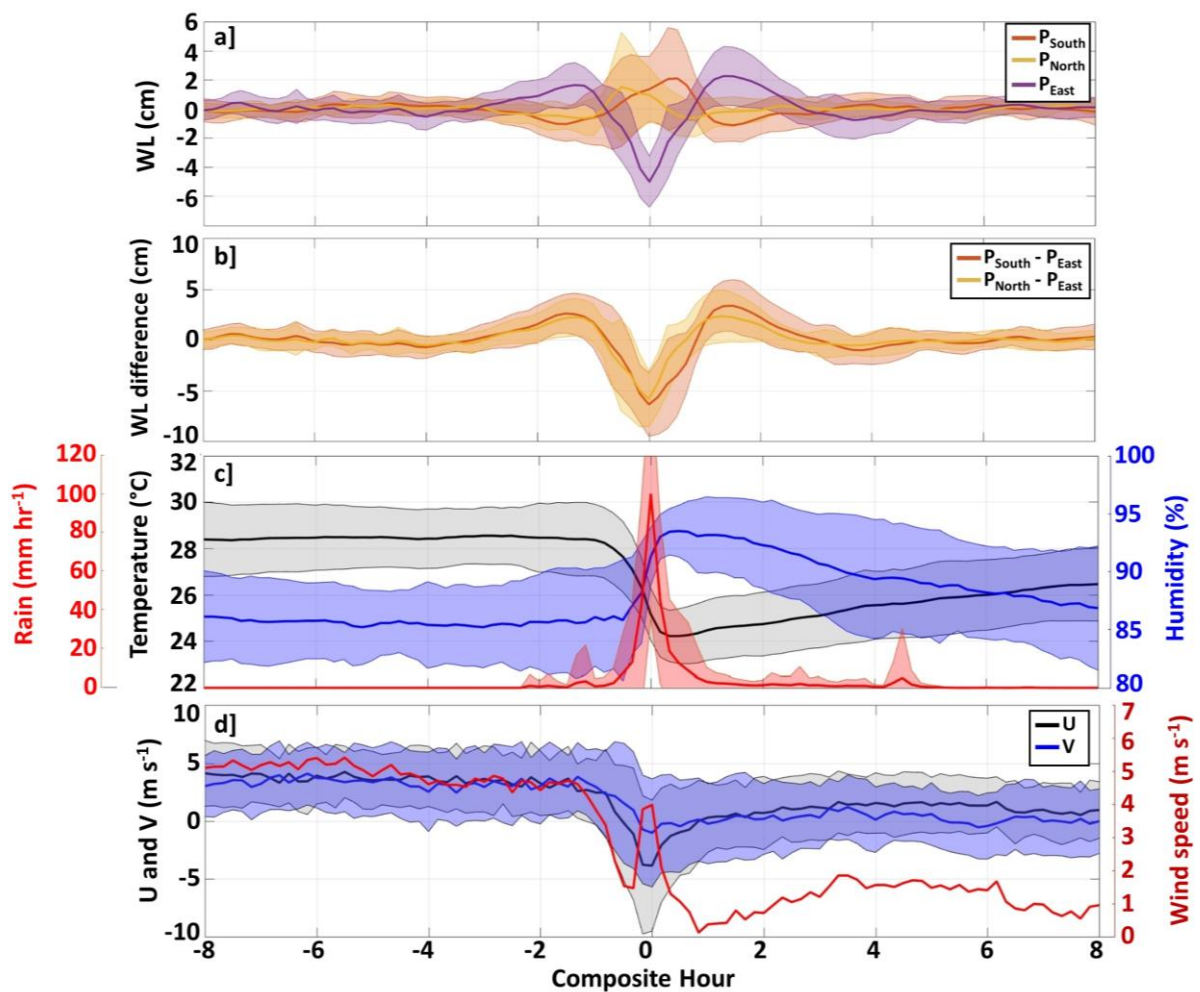
487  
488 As an example, Figure 6c shows the HF WL variations for the particular event that  
489 occurred during the night 09-10 April 2018. Between 08:00 and 10:00 pm, the WL  
490 increased by  $\sim 7$ -8 cm in the eastern part of the lagoon ( $P_{East}$ ) at a simultaneous decrease  
491 of 4-5 cm at  $P_{South}$  and  $P_{North}$ . Thus, this rapid evolution generated a WL difference of 12-  
492 13 cm between the East and the central line of the lagoon joining  $P_{South}$  and  $P_{North}$ . After  
493 10:00 pm, the WL rapidly decreased (increased, respectively) at  $P_{East}$  ( $P_{South}$  and  $P_{North}$ )  
494 to reach a maximum negative (positive) anomaly of -13.5 cm (+10 cm) between 11:00  
495 pm and midnight (Figure 6c). This led to a maximum WL difference of  $\sim 23$  cm between  
496 the eastern and central parts of the lagoon. Subsequently, the WL began to oscillate

497 around its equilibrium value with amplitudes of a few cm. These oscillations,  
498 characterized by a period of  $\sim 2\text{h}45\text{mins}$ , were rapidly dissipated on 10 April after 08:00  
499 am. This  $\sim 12$ -hour duration event, characterized by regular WL free standing-wave  
500 oscillations that are progressively dampened, is typical of a seiche event as frequently  
501 observed in other lakes, lagoons or coastal embayments (e.g. Chapman and Giese, 2001).  
502 For this particular event, the observed standing-wave oscillation period of  $2\text{h}45\text{mins}$  is  
503 in close agreement with the Merian's theoretical period of a seiche oscillation in a  
504 rectangular flat-bottom basin (Chapman and Giese, 2001): considering the larger  
505 dimension of the Lagoon ( $L = 20$  km) and a mean depth ( $H$ ) of 1.3 m, the Merian's  
506 theoretical period value ( $T = \frac{2L}{\sqrt{gH}}$ ) is of  $\sim 3\text{h}$ .

507 In order to better characterize such HF events, and to provide a more robust  
508 description of their main characteristics, a composite analysis was performed. First,  
509 individual HF events were filtered as any event associated with a strong WL increase at  
510 a given lagoon station ( $P_{\text{South}}$ ,  $P_{\text{North}}$ , and  $P_{\text{East}}$ ) and a simultaneous strong WL decrease in  
511 another gauged station. In order to ensure a high confidence level and exclude any  
512 potential false detection, a strong increase/decrease is defined as higher than  $\pm 4$   
513 standard deviations from the mean (Figure 6). Peaks with such high variations occur  
514 less than 0.1% of the time. A total of 44 HF events, significantly impacting at least 2 WL  
515 stations, were detected. Interestingly, more than 75% (34 on 44) of these events were  
516 associated with a strong WL minimum in the eastern part of the lagoon at  $P_{\text{East}}$ , as also  
517 observed in Figure 6c. In terms of seasonality, about 85% of the 44 HF events took place  
518 during the dry season between February and June and none of them between August  
519 and September.

520 Second, since the lagoon is elongated in East-West direction and seiche  
521 phenomena are expected to more likely develop along the elongated direction, we  
522 selected only HF events characterized by a significant WL minimum at  $P_{\text{East}}$ .  
523 Furthermore, after visual inspections, we retained 32 events characterized by similar  
524 evolutions in meteorological parameters. Figure 7a displays the composite analysis of  
525 the WL evolution for these 32 events, obtained by centering each event at the time the  
526 WL minimum at  $P_{\text{East}}$  was observed ( $t=0\text{h}$  in Figure 7). On average, about 3 hours before  
527 the start of the seiche, the WL gently rises by 2 cm to the East and decreases by  $\sim 1$  cm at  
528  $P_{\text{South}}$  and  $P_{\text{North}}$ . Note that the seiche is triggered at time  $t=-1.5\text{h}$ , when the WL starts to  
529 decrease (increase respectively) at  $P_{\text{East}}$  ( $P_{\text{South}}$  and  $P_{\text{North}}$ ). The WL anomaly reaches its

530 minimum value (-5 cm) at  $P_{East}$  at  $t=0h$ , while maximum WL anomalies ( $\sim 2$  cm) are  
 531 observed at  $P_{North}$  and  $P_{South}$  at  $t=-0.5h$  and  $t=+0.5h$  respectively. Then, as observed for  
 532 the individual event shown in Figure 6, the WL oscillates with inverse anomalies  
 533 between  $P_{East}$  and  $P_{North}/P_{South}$  (Figure 7a), with an oscillation period of  $\sim 3h-3h30$ . The  
 534 dissipation is much faster than the single event analyzed in Figure 6, due to the averaging  
 535 of 32 events that can be characterized by slightly different periods and amplitudes.  
 536



537  
 538 *Figure 7. Composite analysis of the high-frequency seiche events and associated atmospheric parameters. a) Averages of*  
 539 *water-level (WL, in cm) evolution in the Nokoué Lagoon ( $P_{South}$ ,  $P_{North}$  and  $P_{East}$ ) for the 32 high-frequency events*  
 540 *associated with a maximum negative WL anomaly at  $P_{East}$  at  $t = 0$ . b) Mean water-level differences between  $P_{South}$  and*  
 541  *$P_{East}$  and between  $P_{North}$  and  $P_{East}$ . c) Mean temporal variations of air-temperature (in  $^{\circ}C$ , black line), air-humidity (in %, blue line)*  
 542 *and rain (in mm/hr, red line). d) Mean temporal variations of wind velocity components (in black and blue, left*  
 543 *axis) and wind speed (in red, right axis). Color shading correspond to  $\pm 1$  standard deviation around the means. In order*  
 544 *not to overload the figure, standard deviations are not shown for wind speed in c).*

545  
 546 Finally, in order to better understand the forcing mechanisms involved in the  
 547 seiche generation, a composite analysis of some key meteorological parameters was

548 performed (Figure 7c-d). Leading up to the seiche triggering, atmospheric conditions are  
549 relatively stable with on average an air temperature of  $\sim 28.5^{\circ}\text{C}$ , a humidity of  $\sim 85\%$ ,  
550 and no rain (Figure 7c). The wind is also regular, blowing towards the Northeast (zonal  
551 and meridional components are equal and positive) with a mean speed of  $4\text{-}5\text{ m s}^{-1}$   
552 (Figure 7d). This wind regime tends to accumulate water in the Northeast/East of the  
553 lagoon as observed in Figure 7a. At the start of the seiche ( $t=-1.5\text{h}$ ) the wind suddenly  
554 decreases and progressively reverses (Figure 7d). At  $t=0$ , when the WL is minimum at  
555  $P_{\text{East}}$ , the wind blows towards the West-Southwest with a mean speed of  $\sim 4\text{ m s}^{-1}$  (Figure  
556 7d). This strong and rapid wind inversion is thus the main forcing mechanism of the  
557 seiche, causing the displacement of the water from the East to the West and initiating  
558 the WL oscillations. After this maximum wind inversion, the wind progressively blows  
559 again towards the Northeast but with a very weak intensity ( $< 2\text{ m s}^{-1}$ ). Interestingly,  
560 during the seiche event the air temperature suddenly drops by  $4\text{-}5^{\circ}\text{C}$ , the humidity  
561 increases to reach an average value of  $93\%$  and very strong rain events are observed  
562 (Figure 7c). These showers of up  $\sim 100\text{ mm/h}$  rainfall have a duration of  $30\text{-}60\text{ mn}$ .  
563 These patterns are likely related to the passage of fast-moving squall-lines,  
564 characterized by strong pressure jumps and downdraft winds, with short but intense  
565 rainfalls (e.g. Omotosho, 1984; 1985; Schrage and Fink, 2007). Interestingly, the  
566 seasonal variation of the number of squall-lines in West African coastal regions, shows a  
567 bi-modal distribution with a strong maximum in March-June and almost no squall-line in  
568 July-September (Omotosho, 1984; 1985). Both the number of squall-lines and the  
569 number of seiche events show similar seasonal variations ( $85\%$  of the seiche events  
570 were observed in February and June and none in August-September), which strongly  
571 suggests that the passage of these atmospheric disturbances (squall-lines) are likely  
572 responsible of the observed seiche phenomena.

573

#### 574 **4. Discussion**

575 As noted by Ekeu-Wei (2018), floods are one of the most devastating natural hazards  
576 in West Africa, increasing in frequency, magnitude and impact in recent decades (Aerts et al.,  
577 2014; Di Baldassarre et al., 2010). Flood in West-Africa is thus a growing issue and various  
578 political or economic capitals are concerned by flooding, in particular due to their proximity  
579 from coastal lagoons fed by important watersheds (e.g. Lagos in Nigeria, Cotonou in Benin,  
580 Lomé in Togo, Abidjan in Ivory Coast, etc.). Local governments therefore need information

581 to implement appropriate flood management measures. However, the acquisition and  
582 maintenance of environmental and climate observation networks in these developing regions  
583 is very challenging despite their vulnerability to climate variability and change (Ampadu et  
584 al., 2013; Eku-Wei, 2018 ; Dinku, 2019 ; Brocca et al., 2020). As such, WL timeseries in  
585 West-African lagoons are rare or non-existent. Results presented in this study, which are  
586 based on several 2-year timeseries of WL in the Nokoué Lagoon in Benin, are therefore  
587 unique in West-Africa and provide important information on the hydrological functioning of  
588 this coastal lagoon for the future implementation of flood early warning system.

589 In particular, this study complemented previous limited studies (Le Barbé et al., 1983;  
590 Djihouessi and Aina, 2018), highlighting the main roles of river runoffs, tides and winds in  
591 the WL variations of Nokoué Lagoon. Observed low-frequency subtidal WL variations of  
592 ~0.8-0.9 m are the result of the importance of continental water inflow and the lagoon's  
593 evacuation capacities, which depend on the ocean level. At regional scale, the WL has only  
594 been measured in the Ebrié Lagoon (Ivory Coast) for 1-year in 1952. This lagoon also showed  
595 an increase of 50 cm during watershed flooding in October-November (Varlet, 1978; Durand  
596 and Guiral, 1994). In Nokoué Lagoon, our results suggested a 1-month delay between  
597 maximum rainfall in the catchment basin and the maximum WL in the lagoon, which is  
598 encouraging to elaborate an operational seasonal flood forecasting system in the lagoon from  
599 rainfall observations.

600 Our study also suggests that such forecasting system has to take into account tide  
601 forcing. The interaction of M2 and S2 tidal constituents through non-linear bottom friction  
602 and river interaction resulted in a pronounced fortnightly-period oscillation of lagoon WL, as  
603 expected from one-dimensional simplified models (e.g. Hill, 1994; MacMahan et al., 2014).  
604 Tides are strongly attenuated, with a main semidiurnal (M2+S2) tidal amplitude decreasing  
605 from 30-90 cm in the ocean to ~1-3 cm in the Nokoué Lagoon (see Table 2 and also  
606 Zandagba et al., 2016). The tidal signal is thus altered by the frictional channel that acts as a  
607 dynamic low-pass filter (Kjerfve and Magill, 1989) and the Nokoué Lagoon can be classified  
608 as a choked coastal lagoon (Kjerfve, 1986) with a choking coefficient varying with the season  
609 and ocean tide amplitude (Table 3).

610 Based on Stigebrandt (1980), many studies have explained choking conditions using a  
611 simple one-dimensional model (e.g. Rydberg and Wickbom, 1996), where the response of the  
612 WL within the lagoon ( $\eta_{lagoon}$ ) to the ocean sea-level forcing ( $\eta_{ocean}$  and M2 tide) and a  
613 variable freshwater supply ( $Q_{river}$ ) is given by:

614

615 
$$\frac{d\eta_{lagoon}}{dt} = P \frac{\eta_{ocean} - \eta_{lagoon}}{\sqrt{|\eta_{ocean} - \eta_{lagoon}|}} + S \quad (1)$$

616 where the parameters characterizing the choking conditions are (Stigebrandt, 1980)

617 
$$P = \frac{hl}{A\sqrt{1+\lambda}} \sqrt{\frac{2gT^2}{a_{ocean}}} \quad \lambda = 2\kappa \frac{L}{h} \quad \text{and} \quad S = \frac{Q_{river}T}{Aa_{ocean}}$$

618  
 619 with  $g = 9.81 \text{ m/s}^2$  is the gravitational acceleration;  $T = 12.42$  hours and  $a_{ocean} = 0.5$  m, are the  
 620 M2 tidal period and amplitude in the ocean, respectively;  $\kappa \sim 0.003$  is a friction coefficient  
 621 used in quadratic friction laws (e.g. Robinson et al., 1983; Stigebrandt and Molvær, 1988;  
 622 Sternberg, 1968; Rydberg and Wickbom, 1996);  $A = 170 \text{ km}^2$  is the lagoon area,  $L = 4000$  m  
 623 the length of the Cotonou channel,  $l = 280$  m its breadth, and  $h = 3$  m its depth. The river  
 624 discharge,  $Q_{river}$ , is poorly known but estimated climatologies show it varies from  $\sim 50 \text{ m}^3 \text{ s}^{-1}$   
 625 in low-water season to  $\sim 800 \text{ m}^3 \text{ s}^{-1}$  during flood period (Figure 2).  
 626

627 *Table 3. Tidal choking coefficients (in bold) obtained from average semidiurnal tidal amplitudes observed in the ocean*  
 628 *( $a_{ocean}$ ) and Nokoué Lagoon ( $a_{lagoon}$ ), and from theoretical results from Equation 1 (Stigebrandt, 1980) for different*  
 629 *hydrological periods (dry and wet seasons) and tidal characteristics (spring and neap tides).  $a_{lagoon}$  was obtained from*  
 630 *Table 2, averaging semidiurnal tidal amplitudes (AD2) at the 3 stations located in Nokoué Lagoon ( $P_{South}$ ,  $P_{North}$ ,  $P_{East}$ ).*

	Observations			Theoretical (Stigebrandt, 1980)		
	$a_{ocean}$ (cm)	$a_{lagoon}$ (cm)	$C_c = \frac{a_{lagoon}}{a_{ocean}}$	$C_c$	$P$	$S$
	<i>Dry Season (<math>Q_{river} = 50 \text{ m}^3 \text{ s}^{-1}</math>)</i>					
<i>Spring Tide</i>	94.2	4.0	<b>0.04</b>	<b>0.06</b>	0.34	0.01
<i>Neap Tide</i>	36.0	2.8	<b>0.08</b>	<b>0.09</b>	0.54	0.04
	<i>Wet Season (<math>Q_{river} = 800 \text{ m}^3 \text{ s}^{-1}</math>)</i>					
<i>Spring Tide</i>	95.3	1.4	<b>0.01</b>	<b>0.02</b>	0.33	0.22
<i>Neap Tide</i>	28.0	1.3	<b>0.05</b>	<b>0.06</b>	0.62	0.75

631  
 632 In this model, tidal choking depends at first order upon the geometrical characteristics  
 633 of the lagoon and channel including friction effects (e.g. Stigebrandt, 1980; Hill, 1994;  
 634 MacMahan et al., 2014). River outflows plays an additional role in modifying both the mean  
 635 lagoon WL and the tidal amplitude and phase (Stigebrandt, 1980). Given the lagoon and river  
 636 discharge characteristics, we obtain  $\lambda \sim 8$  indicating a strong control of tidal choking by  
 637 bottom friction.  $P$  varies from 0.3 for spring semidiurnal tides to 0.6 for neap tides (Table 3).  
 638 Interestingly, because of extreme hydrological variability,  $S$  varies from 0.01 in dry season to  
 639 0.8 in wet season (Table 3), implying a strong influence of river discharge for the choking  
 640 process. Following Stigebrandt (1980; see his Table 1), the predicted choking coefficient

641 varies from 0.02 to 0.09 (Table 3). These results only slightly differ from our estimates (Table  
642 3), in particular because river inflow is poorly known. This good agreement shows that this  
643 simple model is able to explain the observed choking conditions and its strong seasonal and  
644 fortnightly variability.

645 Also, for the considered river outflows ( $50$  and  $800 \text{ m}^3 \text{ s}^{-1}$ ) the Stigebrandt's (1980)  
646 theory predicts a similar tidal asymmetry in the lagoon, with an ebb duration  $\sim 35$  mn longer  
647 than the flood. This is in agreement with what we observed during dry season (30-45 mn), but  
648 the observed ebb-flood asymmetry was stronger during flood period. The expected phase  
649 delay between high water in the ocean and in the lagoon is predicted to be of 1.5-3 hours  
650 (longer phase shifts for stronger river outflows), in agreement with the values observed in  
651 Section 3.3b. Furthermore, Stigebrandt (1980) suggested from his theory that the mean WL in  
652 the lagoon would increase by 5 cm in low-water period and  $\sim 80$  cm during flood season,  
653 which is very close to our observations (Figure 2). These comparisons between observed and  
654 predicted values from the Stigebrandt's (1980) theory at different timescales are very  
655 promising for using this simplified one-dimensional models to predict WL in Nokoué Lagoon  
656 from river discharge data and tidal constituents. Implementing a forecasting system was  
657 beyond the scope of the present study, but this problem and approach will deserve future  
658 studies.

659 Finally, as shown in Section 3.4, the HF WL acquisition rates allowed us to highlight  
660 the occurrence of seiches in Nokoué Lagoon and to provide their main characteristics. These  
661 HF events, forced by the passage of fast-moving squall lines, are characterized by typical WL  
662 oscillations of  $\pm 5$ -10 cm. Seiches are commonly observed in large lakes or lagoon in the  
663 World (e.g. Chapman and Giese, 20021). However, due to the lack of continuous WL  
664 monitoring, these HF events have been only marginally documented in some lakes of Central  
665 and East Africa (e.g. Beauchamp, 1939; 1953; Jollyman, 1955; Fish, 1957; Ward, 1959). In  
666 West-Africa, only Varlet (1978) mentioned the occasional existence of damped oscillations in  
667 the Ebrié Lagoon whose amplitude could reach 10 cm and whose period was about thirty  
668 minutes. He also noted that in 1952, a tornado produced a momentary rise of 5-15 cm in the  
669 Ebrié lagoon. Our study, based on a robust statistical analysis, provides an unprecedented  
670 description of the seiche phenomenon in an African coastal lagoon. These results provide  
671 useful metrics to validate barotropic shallow-water models, that in turn could be used to better  
672 understand seiche dynamics in Nokoué Lagoon. They also suggest that, to be exhaustive,  
673 flood forecasting system should incorporate or parameterize seiche oscillations in Nokoué  
674 Lagoon.

675

## 676 **5. Conclusion**

677 The lagoon WL exhibits strong variability in 4 main frequency bands. First, a low-  
678 frequency variability is directly associated with the seasonal variation of rainfall and  
679 river discharge that causes the WL in the lagoon to increase by 0.9 m between low and  
680 high water periods. Some interannual variability was observed, related to variations of  
681 rainfall over the watershed and associated river discharge, but the lack of available  
682 contemporary hydrological and meteorological data prevents any further diagnostics.

683 Second, we documented the propagation and interaction of oceanic tidal  
684 constituents within the Cotonou channel and Nokoué Lagoon. Fortnightly frequency  
685 variations of the mean WL are observed in the lagoon with the highest high-waters  
686 observed during spring tides and the lowest low-waters during neap tides. Amplitudes  
687 of the fortnightly variations are much higher (10-15 cm) during the wet season. A strong  
688 attenuation of the tidal range within the Cotonou channel is observed, as well as the  
689 general flood-dominated character of the lagoon. On average, semi-diurnal (diurnal,  
690 respectively) tidal amplitudes decreases from ~70 cm (15 cm) in the ocean to ~2-3 cm  
691 (<2 cm) within the lagoon. Thus, the relatively long Cotonou channel, that connects the  
692 Nokoué Lagoon to the ocean, acts as a natural low-pass filter that reduces tidal effect in  
693 the lagoon but increase the fortnightly component, and more particularly during wet  
694 season when river discharge is high.

695 Third, we observed higher frequency WL variability, characterized by periods  
696 shorter than 5 h. Most of these energetic events are observed during the dry season, and  
697 are associated with typical WL variations of 5-10 cm. These HF patterns correspond to  
698 wind-forced seiches associated with the passage of fast-moving squall-lines. The  
699 perturbation of the persistent southwest winds by the passage of these atmospheric  
700 disturbances leads to the development of seiches with a period of ~3 h. During these  
701 events, that are rapidly dissipated, heavy rainfalls are observed and the air temperature  
702 drops on average by 5°C.

703 The observations and diagnostics of this study contribute to a better  
704 understanding of the dynamics of the Nokoué Lagoon and may be used to inform an  
705 improved management of flood risks of the adjacent low-lying coastal cities. Indeed, our  
706 study shows that in order to be realistic, a flood early warning system should not only  
707 consider the hydrological regime of the Sô and Ouémé rivers, but also the propagation

708 and non-linear interactions of the ocean tide that produces significant WL fluctuations of  
709 Nokoué Lagoon, in particular at fortnightly periods during flood season (Figures 2-3). In  
710 a second step, this flood warning system should also include seiches that give rise to  
711 high frequency WL oscillations and can cause additional surges.

712

### 713 **Acknowledgments.**

714 Field campaigns and instrumentation were supported by IRD, IRHOB and ANR @RAction  
715 chair medLOC (ANR-14-ACHN-0007-01–T.Stieglitz). V. OKPEITCHA was funded by  
716 OmiDelta project of the Embassy of the Netherlands in Benin, through a scholarship grant of  
717 the National Institute of Water (INE). This work is a contribution to the « JEA1 SAFUME »  
718 project funded by IRD. Special thanks to the members and crew participating to the  
719 deployment and recovery of the sensors, and in particular to Joseph AZANKPO.

720

721

722 **References.**

- 723 Adadedjan, D., Makponse, E., Hinvi, L.C., Lalèyè. P., 2017. Données préliminaires sur la  
724 diversité du zooplancton du lac Nokoué (Sud-Bénin). *Journal of Applied Biosciences*  
725 115, 11476–11489.
- 726 Adite, A., and Winemiller, K.O., 1997. Trophic ecology and ecomorphology of fish  
727 assemblages in coastal lakes of Benin, West Africa. *Écoscience* 4 (1), 6-23.
- 728 Adite, A., ImorouToko,I., Gbankoto, A., 2013. Fish Assemblages in the Degraded  
729 Mangrove Ecosystems of the Coastal Zone, Benin, West Africa: Implications for  
730 Ecosystem Restoration and Resources Conservation. *Journal of Environmental*  
731 *Protection* 4 (12), 1461-1475.
- 732 Adjahouinou, D.C., Liady, N.D., Fiogbe, E.D., 2012. Diversité phytoplanctonique et niveau  
733 de pollution des eaux du collecteur de Dantokpa (Cotonou-Bénin), *Int. J. Biol. Chem.*  
734 *Sci.* 6 (5), 1938-1949.
- 735 Adjahouinou, D.C., Yehouenou, B., Fiogbe, E.D., Liady, M.N.D., 2014. Caractérisation  
736 bactériologique des eaux résiduaires brutes de la ville de Cotonou (Benin). *Journal of*  
737 *Applied Biosciences* 78, 6705 – 6713.
- 738 **Aerts, J. C., Botzen, W. W., Emanuel, K., Lin, N., De Moel, H., Michel-Kerjan, E. O., 2014.**  
739 **Evaluating flood resilience strategies for coastal megacities. *Science*, 344(6183), 473-**  
740 **475.**
- 741 Ahouangan, M.B.D., Djaby, B., Ozer, P., Hountondji, Y.C., Thiry, A., De Longueville, F.,  
742 2014. Adaptation et résilience des populations rurales face aux catastrophes  
743 naturelles en Afrique subsaharienne. Cas des inondations de 2010 dans la commune  
744 de Zagnanado, Bénin. In: Ballouche, A. & Taïbi, N. A. (Eds.), *Eau, milieux et*  
745 *aménagement. Une recherche au service des territoires.* Presses de l'Université  
746 d'Angers, Angers, France, pp. 265-278.
- 747 Ahokossi, Y., 2018. Analysis of the rainfall variability and change in the Republic of  
748 Benin (West Africa), *Hydrological Sciences Journal* 63 (15-16), 2097-2123.
- 749 Aina, M. P., Degila, H., Chikou, A., Adjahatode, F., Matejka, G., 2012a. Risk of intoxication  
750 by heavy metals (Pb, Cd, Cu, Hg) connected to the consumption of some halieutic  
751 species in lake Nokoué: case of the *Penaus schrimps* and the *Sarotherodon*  
752 *Melanotheron*. *British Journal of Science* 5 (1), 104-118.

753 Aina, M.P., Djihouessi, B., Vissin E.W., Kpondjo, N.M., Gbèdo, V., Sohounhloué K.C.D.,  
754 2012b. Characterization of the domestic wastewaters and dimensionality of a pilot  
755 treatment station by lagooning at Abomey Calavi city- Benin. *J. Engineering Sci.* 1 (1),  
756 45-50.

757 Allersma, E., Tilmans, W.M.K., 1993. Coastal Conditions in West Africa: A Review. *Ocean*  
758 *and Coastal Management* 19, 199-240.

759 Ampadu, B., Chappell, N. A., Kasei, R. A., 2013. Rainfall-Riverflow modelling approaches:  
760 making a choice of data-based mechanistic modelling approach for data limited  
761 catchments: A review. *Canadian Journal of Pure and Applied Sciences*, 7(3), 2571-  
762 2580.

763 Aubrey, D.G., Speer, P.E., 1985. A study of non-linear tidal propagation in shallow  
764 inlet/estuarine systems Part I: Observations. *Estuarine Coastal Shelf Science* 21, 185–  
765 205.

766 Beauchamp, R.S.A., 1939. Hydrology of Lake Tanganyika. *Int. Rev. ges. Hydrobiol.* 39,  
767 316-353.

768 Beauchamp, R.S.A., 1953. Hydrological data from Lake Nyasa. *J. Ecol.* 41, 226-239.

769 Biao, E. I., 2017. Assessing the impacts of climate change on river discharge dynamics in  
770 Ouémé river basin (Benin, West Africa). *Hydrology* 4 (47).

771 Brocca, L., Massari, C., Pellarin, T., Filippucci, P., Ciabatta, L., Camici, S., Kerr, Y.H.,  
772 Fernández-Prieto, D., 2020. River flow prediction in data scarce regions: soil moisture  
773 integrated satellite rainfall products outperform rain gauge observations in West  
774 Africa. *Scientific Reports*, 10(1), 1-14.

775 Brookes, J., Povilanskas, R., Khokhlov, V., 2018. Assessing, quantifying and valuing the  
776 ecosystem services of coastal lagoons. *Journal for Nature Conservation* 44, 50-65.

777 Carrere L., Lyard, F., Cancet, M., Guillot, A., Picot, N., 2016. FES 2014, a new tidal model -  
778 Validation results and perspectives for improvements, presentation to ESA Living  
779 Planet Conference, Prague 2016.

780 Chapman, D. C., Giese, G.S., 2001. Waves: Seiches, in *Encyclopedia of Ocean Sciences* 5,  
781 edited by J. H. Steele, K. K. Turekian, and S. A. Thorpe, pp. 2724–2731, Academic,  
782 London.

783 Choplin, A., 2019. Produire la ville en Afrique de l’Ouest : le corridor urbain de Accra à  
784 Lagos. *L’Information géographique* 83 (2), 85–103.

785 Colleuil B. (1987). Le complexe lagunaire du Lac Nokoué et de la lagune de Porto-Novo  
786 (Bénin). In : Burgis M.J. (ed.), Symoens J.J. (ed.), Gac Jean-Yves (coord.). African  
787 wetlands and shallow water, Paris : ORSTOM, (211), 188-196.

788 Colvin, J., Lazarus, S., Splitt, M., Weaver, R., and Taeb, P. 2018. Wind driven setup in east  
789 central Florida's Indian River Lagoon: Forcings and parameterizations. *Estuarine,  
790 Coastal and Shelf Science*, 213, 40-48.

791 Courtier, A., 1938. Marées. Service Hydrographique de la Marine, Paris, available at :  
792 <https://journals.lib.unb.ca/index.php/ihr/article/download/27428/1882520184>  
793 (last access: 24 December 2020).

794 Di Baldassarre, G., Montanari, A., Lins, H., Koutsoyiannis, D., Brandimarte, L., Blöschl, G.,  
795 2010. Flood fatalities in Africa: from diagnosis to mitigation. *Geophysical Research  
796 Letters*, 37(22).

797 Dinku, T., 2019. Challenges with availability and quality of climate data in Africa. In  
798 *Extreme hydrology and climate variability*. Elsevier. 71-80.

799 Djihouessi, M.B., Aina, M.P., Kpanou, B.V., Kpondjo, N., 2017. Measuring the Total  
800 Economic Value of Traditional Sand Dredging in the Coastal Lagoon Complex of  
801 Grand-Nokoue (Benin). *Journal of Environmental Protection* 8, 1605-1621.

802 Djihouessi, M.B., Aina, M.P., 2018. A review of hydrodynamics and water quality of Lake  
803 Nokoué: current state of knowledge and prospects for further research. *Reg. Stud.  
804 Mar. Sci.* 18, 57–67.

805 Djihouessi, M.B., Djihouessi, M.B., Aina, M.P., 2019. A review of habitat and biodiversity  
806 research in Lake Nokoué, Benin Republic: Current state of knowledge and prospects  
807 for further research. *Ecohydrology and Hydrobiology* 18(1), 1-15.

808 Duck, R. W., da Silva, J. F., 2012. Coastal lagoons and their evolution: a  
809 hydromorphological perspective. *Estuarine, Coastal and Shelf Science* 110, 2-14.

810 Durand, J. R., Guiral, D., 1994. *Hydroclimat et hydrochimie*. In : *Environnement et  
811 ressources aquatiques de Côtes d'Ivoire. Tome 2 : les milieux lagunaires*, Durand J. R.,  
812 Dufour P., Guiral D. et Zabi S. G. F. éditeurs. Editions de l'ORSTOM, Paris, 59-90.

813 Ekeu-Wei, I. T. (2018). Evaluation of hydrological data collection challenges and flood  
814 estimation uncertainties in Nigeria. *Environment and Natural Resources Research*,  
815 8(2), 44-54.

816 Evtimova, V. V., Donohue, I., 2016. Water-level fluctuations regulate the structure and  
817 functioning of natural lakes. *Freshwater Biology* 61, 251–264.

818 Fish, G.R., 1957. *A Seiche Movement and Its Effect on the Hydrology of Lake Victoria.*  
819 *Fish. Publs Colon. Office, London* 10, 1-68.

820 Friedrichs, C.T., Aubrey, D.G., 1988. Non-linear tidal distortion in shallow well-mixed  
821 estuaries: a synthesis. *Estuarine, Coastal and Shelf Science* 27 (5), 521-545.

822 Gallo, M.N., Vinzon, S.B., 2005. Generation of overtides and compound tides in Amazon  
823 estuary. *Ocean Dynamics* 55, 441–448.

824 Glenne, B., Simensen, T., 1963. Tidal current choking in the landlocked fjord of  
825 NordÅsyatnet. *Sarsia*, 11(1), 43-73.

826 Gnohossou, P. M., 2006. La faune benthique d'une lagune ouest Africaine (le lac Nokoue  
827 au Bénin), diversité, abondance, variations temporelles et spatiales, place dans la  
828 chaîne trophique. Doctorat, Institut National Polytechnique de Toulouse, France, 184  
829 p.

830 Gu, G., Adler, R.F, 2004. Seasonal evolution and variability associated with the West  
831 African monsoon system. *Journal of Climate* 17, 3364– 3377.

832 Guo, L., van der Wegen, M., Jay, D.A., Matte, P., Wang, Z.B., Roelvink, D., He, Q., 2015.  
833 River-tide dynamics: Exploration of nonstationary and nonlinear tidal behavior in the  
834 Yangtze River estuary. *Journal of Geophysical Research Oceans* 120, 3499–3521.

835 Guo, L., Wang, Z. B., Townend, I., He, Q., 2019. Quantification of tidal asymmetry and its  
836 nonstationary variations. *Journal of Geophysical Research: Oceans* 124, 773–787.

837 Guragai, B., Hashimoto, T., Oguma, K., Takizawa, S., 2018. Data logger-based  
838 measurement of household water consumption and micro-component analysis of an  
839 intermittent water supply system. *Journal of Cleaner Production* 197 (1), 1159-1168.

840 Hill, A.E., 1994. Fortnightly tides in a lagoon with variable choking. *Estuar. Coast. Shelf*  
841 *Sci.* 38, 423-434.

842 Houéménou, H., Tweed, S., Dobigny, G., Babic, M., Mama, D., Alassane, A., Silmer, R., Ruy,  
843 S., Chaigneau, A., Socohou, A., Dossou, H.-J., Badoum, S., Leblanc, M., 2020. Degradation  
844 of groundwater quality in expanding cities in West Africa. A case study of the  
845 unregulated shallow aquifer in Cotonou. *Journal of Hydrology* 582, 124438.

846 Hudgins, L., C. A. Friehe, and M. E. Mayer, 1993. Wavelet transforms and atmospheric  
847 turbulence. *Phys. Rev. Lett.*, 71, 3279–3282.

848 Huffman, G.J., Bolvin, D.T., Braithwaite, D., Hsu, K., Joyce, R., Xie, P., 2014. NASA Global  
849 Precipitation Measurement (GPM) Integrated Multi-Satellite Retrievals for GPM  
850 (IMERG) algorithm theoretical basis Doc., version 4.4. NASA GSFC, 30 pp.

851 Jollyman, W.H., 1955. Tides and seiches in lake Nyasa. *The Nyasaland Journal*, Vol. 8, No.  
852 2, 31-35

853 Kjerfve, B., 1986. Comparative oceanography of coastal lagoons. In: Wolfe DA (ed)  
854 Estuarine Variability. Academic Press, New York, pp 63–81.

855 Kjerfve, B., Magill, K. E., 1989. Geographic and hydrodynamic characteristics of shallow  
856 coastal lagoons. *Marine geology*, 88(3-4), 187-199.

857 Knoppers, B., 1994. Aquatic primary production in coastal lagoons. In Kjerfve, B. (Ed.).  
858 Coastal lagoon processes. Amsterdam, The Netherlands: Elsevier. Elsevier  
859 Oceanography Series 60, 243-285.

860 Lalèyè, P., Philippart, J.C., Poncin, P., 1995. Biologie de la reproduction de deux espèces  
861 de Chrysichthys (Siluriformes, Bagridae) du lac Nokoue et de la lagune de Porto-Novo  
862 au Bénin. *Journal of African Zoology* 109 (3), 213-224.

863 Lalèyè, P., Niyonkuru, C., Moreau, J., Teugels, G.G., 2003. Spatial and Seasonal  
864 Distribution of the Ichthyofauna of Lake Nokoué, Benin, West Africa. *African Journal*  
865 *of Aquatic Sciences*, 28, 151-161.

866 Lalèyè, P., Villanueva, M.C., Entsua-Mensah, M., Moreau, J., 2007. A review of the aquatic  
867 living resources in Gulf of Guinea lagoons with particular emphasis on fisheries  
868 management. *Journal of Afrotropical Zoology*. Proceedings of the Third International  
869 Conference on Africa Fish and Fisheries, Cotonou, Benin, 10–14 November 2003,  
870 Special issue, 123–136.

871 Lawin, A.E., Houngouè, R., N'Tcha M'Po, Y., Houngouè, N.R., Attogouinon, A., Afouda, A.A.,  
872 2019. Mid-Century Climate Change Impacts on Ouémé River Discharge at Bonou  
873 Outlet (Benin). *Hydrology*, 6 (72), <https://doi.org/10.3390/hydrology6030072>

874 Le Barbé, L., Alé, G., Millet, B., Texier, H., Borel, Y., Gualde, R., 1993. Les ressources en  
875 eaux superficielles de la République du Bénin. ORSTOM, Paris, 540 pp.

876 LeBlond, P. H., 1979. Forced fortnightly tides in shallow rivers. *Atmosphere-Ocean*, 17:3,  
877 253-264, doi: 10.1080/07055900.1979.964906

878 Liu, Y., San Liang, X., Weisberg, R. H., 2007. Rectification of the Bias in the Wavelet Power  
879 Spectrum. *Journal of Atmospheric and Oceanic Technology* 24 (12), 2093-2102.

880 Lobo, M.T.M.P.S., de Souza Nogueira, I., Fabris Sgarbi, L., Nunes Kraus, C., de Oliveira  
881 Bomfim, E., Garnier, J., da Motta Marques, D., Bonnet, M.-P., 2018. Morphology-based  
882 functional groups as the best tool to characterize shallow lake-dwelling  
883 phytoplankton on an Amazonian floodplain. *Ecol. Indic.* 95, 579–588.

884 Lyard F., L. Carrere, M. Cancet, A. Guillot, N. Picot, 2021. FES2014, a new finite elements  
885 tidal model for global ocean, in preparation, to be submitted to *Ocean Sciences-*  
886 *Special issue on Tides.*

887 **MacMahan, J., van de Kreeke, J., Reniers, A., Elgar, S., Raubenheimer, B., Thornton, E.,**  
888 **Weltmer, M., Rynne, P., Brown, J., 2014. Fortnightly tides and subtidal motions in a**  
889 **choked inlet. *Estuarine, Coastal and Shelf Science*, 150, 325-331.**

890 Mama, D., Deluchat, V., Bowen, J., Chouti, W., Yao, B., Gnon, B., Baudu, M., 2011.  
891 Caractérisation d'un Système Lagunaire en Zone Tropicale: Cas du lac Nokoué  
892 (Bénin). *Eur. J. Sci. Res.* 56 (4), 516–528.

893 Newton, A., Brito, A.C., Icely, J.D., Derolez, V., Clara, I., Angus, S., Schernewski, G., Inácio,  
894 M., Lillebø, A.I., Sousa, A.I., Béjaoui, B., Solidoro, C., Tosic, M., Cañedo-Argüelles, M.,  
895 Yamamuro, M., Reizopoulou, S., Tseng, H.-C., Canu, D., Roselli, L., Maanan, M., Cristina,  
896 S., Ruiz-Fernández, A.C., de Lima, R.F., Kjerfve, B., Rubio-Cisneros, N., Pérez-Ruzafa, A.,  
897 Marcos, C., Pastres, R., Pranovi, F., Snoussi, M., Turpie, J., Tuchkovenko, Y., Dyack, B.,  
898 2018. Assessing, quantifying and valuing the ecosystem services of coastal lagoons.  
899 *Journal for Nature Conservation* 44, 50-65.

900 N'Tcha M'Po, Y., Lawin, E., Yao, B., Oyerinde, G., Attogouinon, A., Afouda, A., 2017.  
901 Decreasing Past and Mid-Century Rainfall Indices over the Ouémé River Basin, Benin  
902 (West Africa). *Climate* 5 (74).

903 Odountan, O., de Bisthoven, L.J., Koudenoukpo, C., Abou, T., 2019. Spatio-temporal  
904 variation of environmental variables and aquatic macroinvertebrate assemblages in  
905 Lake Nokoué, a RAMSAR site of Benin. *African Journal of Aquatic Science* 44 (3), 219–  
906 231.

907 Okpeitcha, V., Chaigneau, A., Morel, Y., Stieglitz, T., Pomalegni, Y., Sohoun, Z., Mama, D..  
908 Seasonal and interannual variability of salinity in a large West-African lagoon  
909 (Nokoué Lagoon, Benin). Submitted to *Estuarine Coastal and Shelf Science*.

910 Omotosho, J.B., 1984. Spatial and seasonal variations of line squalls over West Africa.  
911 *Arch. Meteorol. Geophys. Bioklimatol. A.* 33, 143 – 150.

- 912 Omotosho, J.B., 1985. The separate contributions of squall lines, thunderstorms and the  
913 monsoon to the total rainfall in Nigeria, *J. Clim.* 5, 543 – 552.
- 914 Percival, D. P., 1995. On estimation of the wavelet variance. *Biometrika*, 82, 619–631.
- 915 Pawlowicz, R., Beardsley, B., Lentz, S., 2002. Classical tidal harmonic analysis including  
916 error estimates in MATLAB using T\_TIDE. *Comput. Geosci.* 28, 929–937.
- 917 Principaud, J.-M., 1995. La pêche en milieu lagunaire dans le sud-est du Bénin. L'exemple  
918 de l'exploitation des acadjas (en danger) sur le lac Nokoué et la basse Sô. In: *Cahiers*  
919 *d'outre-mer*, 192, 48e année. Togo-Bénin, 519-546.
- 920 Pugh, D.T., 1987. Tides, Surges and Mean Sea Level. John Wiley and Sons, New York. 472  
921 pp.
- 922 Ray, R. D., 2007. Propagation of the overtide M4 through the deep Atlantic Ocean.  
923 *Geophysical Research Letters*, 34, L21602, doi:10.1029/2007GL031618.
- 924 Robinson, I.S., Warren, L., Longbottom, J.F., 1983. Sea-level fluctuations in the Fleet, an  
925 English tidal lagoon. *Estuar. Coast. Shelf Sci.* 16, 651-668.
- 926 Rydberg, L., Wickbom, L., 1996. Tidal-choking and bed friction in Negombo Lagoon, Sri  
927 Lanka. *Estuaries* 19e3, 540-547.
- 928 Schrage, J.M., Fink, A.H., 2007. Use of a rain gauge network to infer the influence of  
929 environmental factors on the propagation of quasi-linear convective systems in West  
930 Africa. *Weather and Forecasting* 22, 1016–1030.
- 931 Speer, P.E., Aubrey, D.G., Friedrichs, C.T., 1991. Non-linear hydrodynamics of shallow  
932 tidal inlet/bay systems. In *Tidal Hydrodynamics*, edited by B. B. Parker, pp. 321–339,  
933 John Wiley, Toronto, Canada.
- 934 Sternberg, R. W., 1968. Friction factors in tidal channels with different bed roughness.  
935 *Marine Geology* 6, 243-260.
- 936 Stević, F, Mihaljević, M, Špoljarić, D. 2013. Changes of phytoplankton functional groups  
937 in a floodplain lake associated with hydrological perturbations. *Hydrobiologia* 709,  
938 143– 158.
- 939 Stieglitz, T. C., van Beek, P., Souhaut, M., and Cook, P. G. 2013. Karstic groundwater  
940 discharge and seawater recirculation through sediments in shallow coastal  
941 Mediterranean lagoons, determined from water, salt and radon budgets. *Marine*  
942 *Chemistry*, 156, 73-84.
- 943 Stigebrant, A., 1980. Some aspects of tidal interactions with fjord constrictions. *Estuar.*  
944 *Coast. Shelf Sci.* 11, 151-166.

945 Stigebrandt, A., & Molvær, J. (1988). On the water exchange of Framvaren. *Marine*  
946 *Chemistry*, 23(3-4), 219-228.

947 Sultan, B., and Janicot, S. 2000: Abrupt shift of the ITCZ over West Africa and intra-  
948 seasonal variability. *Geophys. Res. Lett.* 27, 3353–3356.

949 Texier, H., Colleuil, B., Profizi, J.P., Dossou, C., 1980. Le lac Nokoué, environnement du  
950 domaine margino-littoral sud-béninois : bathymétrie, lithofaciès, salinité, mollusque  
951 et peuplements végétaux. *Bull. Inst. Géol. Bass. Aguit.* Bordeaux 28, 115-142.

952 Torrence, C., Compo, G.P., 1998. A Practical Guide to Wavelet Analysis. *Bull. Am. Met. Soc.*  
953 79, 61-78.

954 Valiela, I., 1995. *Marine Ecological Processes*, second ed. Springer-Verlag, New York.

955 Varlet, F., 1978. *Le régime de la lagune Ébrié, Côte-d'Ivoire. Traits physiques essentiels.*  
956 *Paris, Travaux et Documents essentiels de l'Orstom*, 83, 162 pp.

957 Veeda, D., Montagne, R., Araujo, M., 2012. Cross-Wavelet Bias Corrected by Normalizing  
958 Scales, *Journal of Atmospheric and Oceanic Technology* 29 (9), 1401-1408.

959 Ward, P.R.B., 1979. Seiches, tides and wind set-up on Lake Kariba. *Limnol. Oceanogr.* 24,  
960 151-157. 261.

961 Wilson, G.V., Rigby, J.R., Ursic, M., Dabney, S.M., 2016. Soil pipe flow tracer experiments:  
962 1. Connectivity and transport characteristics. *Hydrology processes* 30, 1265-1279.

963 World Bank, 2011. *Inondations au Benin: Rapport d'Evaluation des Besoins Post*  
964 *Catastrophe*. World Bank: Washington, DC, USA. available at :  
965 [http://documents1.worldbank.org/curated/en/750141468208769683/pdf/694130](http://documents1.worldbank.org/curated/en/750141468208769683/pdf/694130ESW0P1240lood0Recovery0Report.pdf)  
966 [ESW0P1240lood0Recovery0Report.pdf](http://documents1.worldbank.org/curated/en/750141468208769683/pdf/694130ESW0P1240lood0Recovery0Report.pdf) (last access: December 24, 2020).

967 Zandagba, J., Moussa, M., Obada, E., Afouda, A., 2016. *Hydrodynamic Modeling of Nokoué*  
968 *Lake in Benin. Hydrology* 2016, 3, 44.

969